Theses and Dissertations

Fall 2010

A computational study of two dimensional laminar premixed combustion of methane and some biofuels

Kevin Langan
University of Iowa

Recommended Citation

Langan, Kevin. "A computational study of two dimensional laminar premixed combustion of methane and some biofuels." MS (Master of Science) thesis, University of Iowa, 2010.
http://ir.uiowa.edu/etd/841.

A COMPUTATIONAL STUDY OF TWO DIMENSIONAL LAMINAR PREMIXED

COMBUSTION OF METHANE AND SOME BIOFUELS

by

Kevin Langan

A thesis submitted in partial fulfillment
of the requirements for the Master of
Science degree in Mechanical Engineering
in the Graduate College of
The University of Iowa

December 2010

Thesis Supervisor: Professor Emeritus Lea-Der Chen

Graduate College
The University of Iowa
Iowa City, Iowa

CERTIFICATE OF APPROVAL

_____

MASTER'S THESIS

_____

This is to certify that the Master's thesis of

Kevin Langan

has been approved by the Examining Committee
for the thesis requirement for the Master of Science
degree in Mechanical Engineering at the December 2010 graduation.

Thesis Committee: _____
                        Lea-Der Chen, Thesis Supervisor

_____
Albert Ratner

_____
H.S. Udaykumar

ACKNOWLEDGMENTS

ABSTRACT

A computational study on two-dimensional laminar premixed combustion has been conducted. A working model was developed that fully coupled a comprehensive chemical kinetic mechanism with computational fluid dynamics in the commercial software program FLUENT. The physical model for the simulations consisted of an adiabatic tube with a constant velocity inlet and an atmospheric pressure outlet. For all cases, the flame waves were shown to be stabilized by the developing boundary layer near the inlet.

The combustion of methane with air was studied in depth and compared with the combustion of three different biofuels: landfill gas and two varieties of syngas. Additionally, combustion with a mixture of O_2 and CO_2 as an oxidizer was proposed as a way to facilitate carbon dioxide capture and sequestration. Flames produced by this combustion technique were then compared with traditional combustion oxidized with air.

Results for methane combustion compared closely with experimental work and one-dimensional numerical work in predicting flame shape, laminar flame speed, and flame thickness. It was shown that the presence of the tube wall affected the flame thickness, but not the laminar flame speed, at sufficiently high inlet velocities. The results from the combustion of landfill gas showed that its laminar flame speed is lower than methane but that its flame shape is similar in nature to that of methane. Simulations of syngas combustion proved to be troublesome for the computational model, which struggled to converge to reasonable solutions, indicating that more work is needed with the numerical modeling method. Results from combustion simulations with the O_2/CO_2 oxidizer revealed that the flame characteristics were affected by the lower thermal diffusivity of the oxidizer, resulting in lower laminar flame propagation speeds and thicker combustion waves. The flame shape remained similar to combustion oxidized with air.

TABLE OF CONTENTS

LIST OF TABLES

Table

LIST OF FIGURES

Figure

LIST OF NOMENCLATURE

A Pre-exponential factor

A_f Area of the flame surface

A_t Cross sectional area of the barrel tube of a Bunsen burner

$D_{m,i}$ Mass diffusion coefficient for species i

$D_{T,i}$ Thermal diffusion coefficient for species i

E Activation energy of the reaction; or total energy

$\vec{F}$ Body forces

F/O Ratio of fuel to oxidant

h_i Sensible enthalpy of species i

h_i^0 Enthalpy of formation of species i

I Unit tensor

$\vec{J}_i$ Diffusive flux of species i

k_f Forward rate reaction constant

k_r Reverse rate reaction constant

K Reaction equilibrium constant

M_i Molecular weight of species i

N_r The number of reactant species

N_p The number of product species

p Static pressure

R Universal gas constant

RR Overall reaction rate

S_L Laminar flame speed

T Temperature

T_{ad} Adiabatic flame temperature

$\vec{v}$ Velocity vector

v_{in} Inlet velocity

V_t Velocity in the barrel tube of a Bunsen burner

w_i Net rate of production of species i

Y_i Mass fraction of species i

α Thermal diffusivity

β Temperature exponent

δ_L Flame wave thickness

$\delta_{L,a}$ Flame thickness at the axis

$\delta_{L,w}$ Flame thickness at the wall

λ Thermal conductivity

ρ Density

ϕ Equivalence ratio

v_i' Stoichiometric coefficient of reactant species i

v_i'' Stoichiometric coefficient of product species i

$\bar{\tau}$ Stress tensor

μ Molecular viscosity

χ_i Chemical symbol for species i

$[\chi_i]$ Molar concentration of species i with chemical symbol χ

CHAPTER 1: INTRODUCTION

1.1 Background

1.1.1 Motivation

The importance of energy use in the world today cannot be understated. Almost every modern convenience and aspect of life requires the use of energy in one way or another. It is the production of this energy and its impact on the global climate that is a topic of much debate, discussion, and research. The majority of the energy that is utilized in the world today is ultimately produced from fossil fuels, specifically crude oil, coal, and natural gas. In fact, more than 80 percent of the energy consumed in the United States in 2009 ultimately came from fossil fuels (U.S. EIA, 2010).

Not only is the current rate of fossil fuel consumption unsustainable from an availability standpoint, it is harmful from an environmental standpoint. It is widely accepted that human activity, particularly the release of carbon dioxide from fossil fuel use, is leading to global climate change. There are many different strategies that can be used in fighting the problems of finite fuel resources and climate change. One strategy is to use the fossil fuels more efficiently. While this is not a cure-all, it does help combat the problem. Another strategy is to develop alternative fuel sources that do not contribute carbon dioxide to the atmosphere and are not limited by finite quantities, hence renewable. An additional strategy is to prevent the carbon dioxide created during energy production from reaching the atmosphere by capturing and sequestering it underground. All three of these strategies are motivation behind the work in this thesis. To use current fuel sources more efficiently, it is necessary to understand the physics governing the ways in which they are used. When examining alternative fuels that are relatively unproven, it is desirable to provide some means of comparing the new fuels with established fuels.

1.1.2 Combustion Basics

For the majority of fuels, the available energy is stored within the chemical bonds of the fuel molecules. This chemical energy contained in the fuel can be extracted in several different ways. The most common method of extracting this energy is through combustion. During combustion, the chemically energetic molecules of the fuel are rapidly oxidized, typically with oxygen in air, to form more stable combustion products while producing large amounts of energy in the form of heat (Moran and Shapiro, 2004).

The combustion process itself is relatively complex. It is an interaction of fluid dynamics, thermodynamics, chemical kinetics, and heat transfer all occurring simultaneously. One simple model to represent the combustion process is an overall stoichiometric equation, which shows a single reaction transforming the reactant species into the product species. An example stoichiometric combustion equation can be seen below for the hydrocarbon fuel methane.

$$CH_4 + 2O_2 \rightarrow CO_2 + 2H_2O \qquad\qquad (1\text{-}1)$$

In reality, the single step reaction depicted in Equation 1-1 does not exist. Instead, numerous different reactions occur in rapid succession, producing and consuming intermediate molecules (Glassman and Yetter, 2008). Ultimately, the products shown in Equation 1-1 are the chief products of the combustion process. Since the overall thermodynamics of process does not depend significantly on the intermediate molecules, overall stoichiometric equations are useful in studying thermodynamic properties of fuels (Glassman and Yetter, 2008).

One useful thermodynamic property of fuels is the adiabatic flame temperature, T_{ad}. The adiabatic flame temperature is the resulting temperature if all the heat from the combustion of a fuel is used to raise the temperature of the combustion products. The value of T_{ad} depends not only on the fuel, but on the oxidizer and the mixture ratio of the fuel and oxidizer. Computing the adiabatic flame temperature involves analyzing the

enthalpies of the reactants and expected products. For more information on the topic, refer to Glassman and Yetter (2008) and Gordon and McBride (1994).

A useful way to classify the mixture ratio of fuel and oxidant is through the equivalence ratio. The equivalence ratio is the ratio of the actual fuel-oxidant ratio to the stoichiometric fuel-oxidant ratio (Moran and Shapiro, 2004). The stoichiometric fuel-oxidant ratio is the mixture of fuel and oxidant that results in complete combustion of the fuel with no leftover oxidant or fuel, as depicted in Equation 1-1. Mathematically, the equivalence ratio is defined as

$$\phi = \frac{F/O}{(F/O)_{st}} \tag{1-2}$$

where ϕ is the equivalence ratio, F/O represents the ratio of fuel to oxidant, and the subscript st denotes the stoichiometric conditions. When equivalence ratio is less than one, then the fuel-oxidant mixture is said to be lean; hence there is excess oxidizer. When the equivalence ratio is greater than one, the fuel-oxidant mixture is said to be rich; hence there is excess fuel. In general, the adiabatic flame temperature of a fuel-oxidant ratio is greatest near stoichiometric conditions (Glassman and Yetter, 2008). In this work, only stoichiometric and lean fuel-oxidant mixtures were studied.

As was mentioned earlier, air is commonly used as the oxidant in combustion. Air mostly consists of oxygen and nitrogen, along with carbon dioxide, argon, water vapor, and other trace elements. For the sake of simplicity, in the work conducted for this thesis, air was assumed to consist of 79% nitrogen and 21% oxygen, on a molecular basis. For the stoichiometric combustion of hydrocarbon fuels with air, the adiabatic flame temperature is on the range of 2100 to 2400 K. When oxidized with pure oxygen, the adiabatic flame temperature of hydrocarbons typically exceeds 3000 K (Glassman and Yetter, 2008).

The numerous reaction steps that occur in a combustion process are important in determining certain characteristics of combustion. Examples include how quickly a

combustion progresses from the reactants to products and the formation of pollutants (Glassman and Yetter, 2008). This is a field of study known as chemical kinetics. In general, the reaction steps in combustion are chain reactions and can be placed into four categories: chain initiation, chain branching, chain propagation, and chain termination. In chain initiation, the fuel molecule reacts to form radicals. Chain branching steps produce more radicals while chain propagation steps maintain the same number of radicals. A chain termination step destroys radicals (Kuo, 2005; Feldick, 2007). All of these reaction steps occur at various points in a combustion process and have a hand in determining the overall characteristics of the combustion.

1.1.3 Laminar Premixed Flames

When a fuel and oxidant mixture is at conditions that will support combustion, the mixture is said to be explosive. If an explosive mixture is ignited, combustion will propagate through the mixture in the form of a wave, often called a flame. In general, a combustion wave can be classified into two categories, detonation and deflagration. A detonation wave is a supersonic wave supported by combustion whereas a deflagration wave is a subsonic wave supported by combustion (Glassman and Yetter, 2008). Combustion in a detonation wave proceeds relatively quickly compared to a deflagration wave. Various conditions, including the physical properties of the combusting apparatus, determine if a flame will occur as a deflagration or detonation (Kuo, 2005).

One type of deflagration wave that has been studied for more than a century is the laminar premixed flame. As the name implies, a laminar premixed flame is a flame wave that propagates in a laminar nature through a homogeneous mixture of fuel and oxidant. A laminar premixed flame wave can be characterized as consisting of two zones, a preheat zone and a reaction zone. Sometimes a third zone is identified, known as the recombination zone, which occurs downstream of the flame wave (Glassman and Yetter,

2008). The general characteristics of temperature, velocity, and reactants as they progress through the combustion wave are depicted in Figure 1-1.
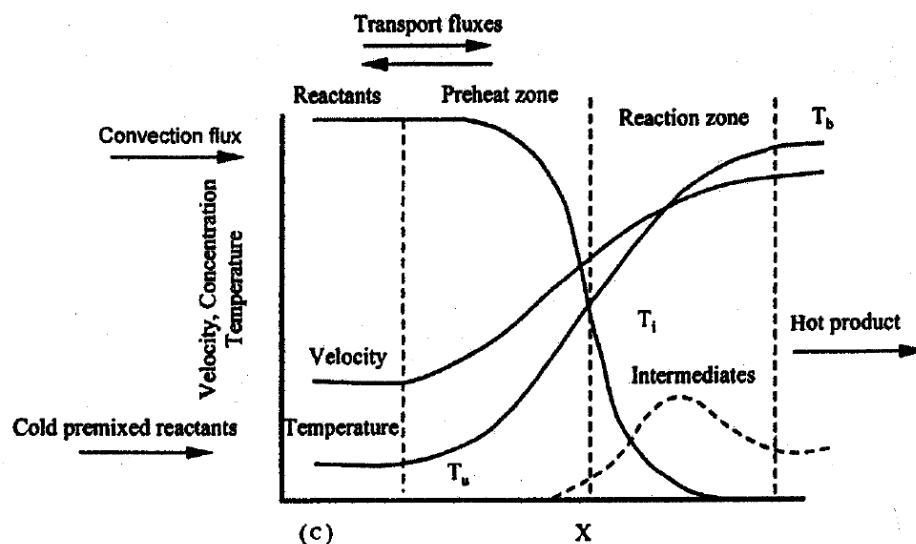
Figure 1-1. Various regimes in a laminar premixed flame wave.

Source: El-Mahallawy, F. and Habik, S.E.D. 2002. *Fundamentals and Technology of Combustion*. Amsterdam: Elsevier.

The flame wave is in essence a balance of the flow of unburned reactants towards the flame zone and the diffusion of radicals and heat from the high temperature reaction zone back towards the preheat region (Glassman and Yetter, 2008). For hydrocarbon combustion, an overview of the reaction proceedings is as follows. In the preheat region, some chain initiating reactions take place as radicals from the reaction zone attack the fuel species. As the fuel moves into the reaction zone, it rapidly decays as it is attacked by the large concentration of *OH* radicals that form at the higher temperatures. Intermediate species are prevalent throughout the reaction zone, as illustrated in Figure 1-1. Near the end of the reaction zone, sufficient *CO* and *OH* concentrations result in the

rapid conversion of CO to CO_2, which accounts for the majority of the heat release in the combustion (Glassman and Yetter, 2008).

Perhaps the most common apparatus for producing laminar premixed flames in a laboratory is the Bunsen burner, which was invented in 1855 (Kuo, 2005). In a Bunsen burner, fuel is mixed with air at the bottom of the burner. The fuel-air mixture then moves through a barrel tube at a velocity low enough to ensure laminar flow. The flame wave then exists in a conical shape just outside the exit of the barrel tube in the ambient atmosphere. A schematic diagram of a Bunsen burner is shown in Figure 1-2.
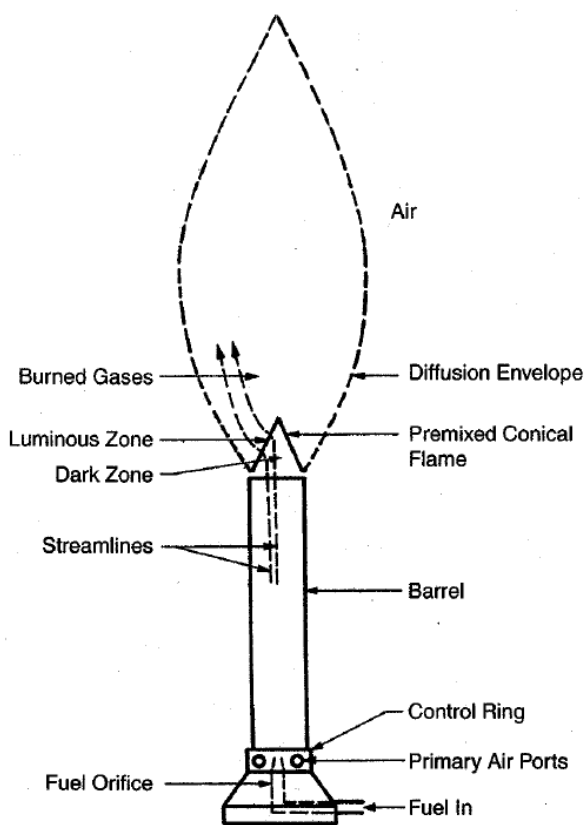
Figure 1-2. Schematic diagram of a laminar premixed flame produced by a Bunsen burner.

Source: Kuo, Kenneth K. 2005. *Principles of Combustion*. New York: John Wiley and Sons.

By the time the fuel-air mixture reaches the top of the barrel tube, it is a homogenous mixture with a laminar parabolic flow profile. In other words, the velocity near the walls of the tube is very low. This low velocity is actually a major factor in the stabilization of the flame (Glassman and Yetter, 2008).

As shown in Figure 1-2, the shape of the flame produced by a Bunsen burner is conical in nature. A schlieren photograph of a laminar premixed flame produced by a Bunsen burner is shown in Figure 1-3.
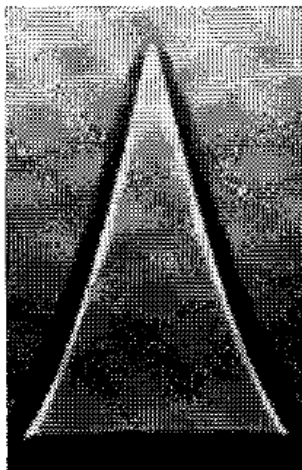
Figure 1-3. Schlieren photograph of a laminar premixed flame produced by a Bunsen burner.

Source: Andersen, J.W. and Fein, R.S. 1950. "Measurement of Normal Burning Velocities of Propane-Air Flames from Shadow Photographs." *Journal of Chemical Physics* 18: 441-443.

In addition to being conical, Figure 1-3 shows that the flame has a slightly concave shape near the outer boundaries of the flame.

Some of the velocity streamlines through the flame surface are shown in Figure 1-1. The general flow pattern in a Bunsen burner flame shows that the unburned fuel-air mixture advances along the axial direction as it approaches the flame. However, near the flame surface, the flow diverges from the axis and moves perpendicularly through the flame surface. The phenomenon is further illustrated in the experimental data shown in Figure 1-4.
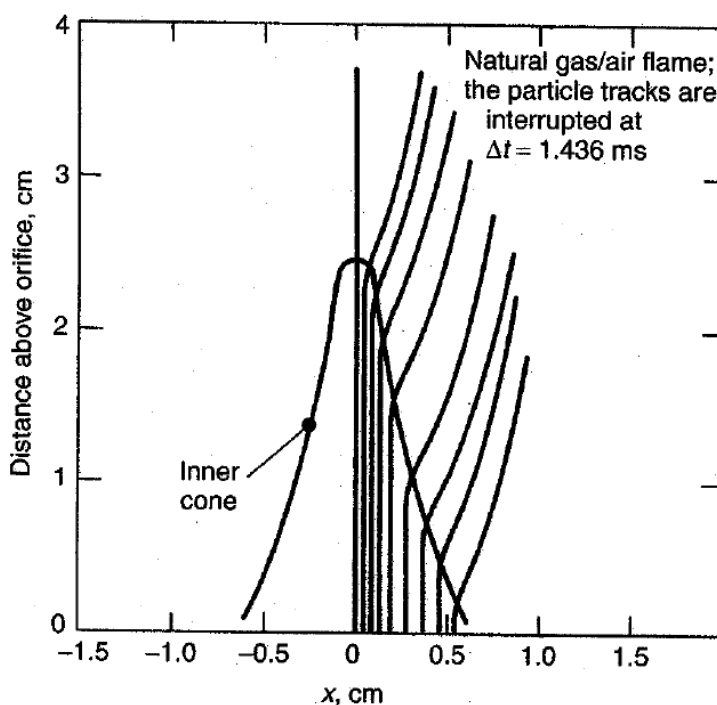
Figure 1-4. Streamlines through a conical laminar premixed flame.

Source: Lewis, B. and von Elbe, G. 1961. *Combustion, Flames and Explosions of Gases (2nd Ed.)*. New York: Academic Press.

The flow patterns through a laminar premixed flame as shown in Figure 1-4 hint at an underlying tendency of unburned gases to propagate normally through the flame wave at a predetermined velocity. Indeed, it has been found through experimental and

numerical work that there is a physical constant in laminar premixed flames known as the laminar flame speed, S_L (Glassman and Yetter, 2008; Kuo, 2005; Lewis and von Elbe, 1961). The laminar flame speed is defined as the velocity of unburned gases through the combustion wave in a direction normal to the flame surface (Kuo, 2005).

For many years, one of the main goals of laminar flame studies was to determine the laminar flame speed of a fuel for a given set of conditions. The Bunsen burner represented one early approach to determining the laminar flame speed of a given fuel-oxidant mixture. Given that the velocity of unburned gases through the combustion wave is uniform, then a simple mass balance at the flame surface results in the following expression for calculating laminar flame speed

$$S_L = V_t \frac{A_t}{A_f} \qquad\qquad (1\text{-}3)$$

where V_t is the velocity in the barrel tube, A_t is the cross sectional area of the barrel tube, and A_f is the area of the flame surface. The problem with this approach often centered around the determination of the flame surface area A_f, which varied depending on which technique was used to visualize the flame. There are many examples of this approach, such as Anderson and Fein (1950) and Ashforth et al. (1950). Other efforts have been taken to directly measure the velocity of the unburned gas flow through the flame surface, such as in Lewis and von Elbe (1961) and more recently by Vagelopoulos (1998).

Other experimental techniques for determining S_L include expanding spherical flames (McLean et al., 1994), and the flat flame burner method (Powling, 1949; Botha and Spalding, 1954). With the advent of increased computational power, experimental techniques for determining S_L gave way to numerical methods for more exact results. Chemical kinetics software, such as CHEMKIN (Kee et al., 2004), can readily compute the theoretical one-dimensional laminar flame speed of a specific fuel-oxidant blend given the parameters of the reaction kinetics for the fuel oxidation. Work such as that

conducted in C. Liu et al. (2010) is based on these numerical techniques. One-dimensional numerical simulations of laminar premixed flames also allow for the analysis of species concentrations throughout the combustion wave. An example of the species and temperature profiles through the flame wave that were produced by a numerical simulation is shown in Figure 1-5.
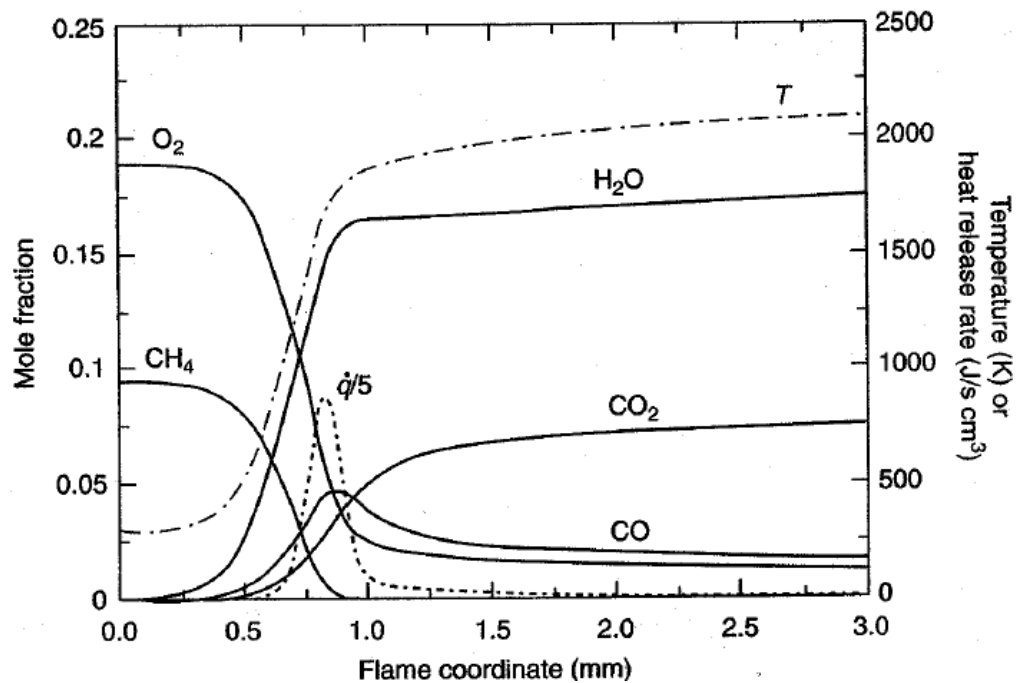
Figure 1-5. Species, temperature, and heat release profiles through a one-dimensional laminar premixed flame. Numerical simulation of stoichiometric methane-air combustion at standard temperature and pressure.

Source: Glassman, I. and Yetter, A. 2008. *Combustion*. Amsterdam: Elsevier.

For many years, the underlying mechanism responsible for the determining laminar flame speed has been studied. Initially, work by Mallard and Le Chatelier theorized that it was heat propagation back through the combustion wave that sustained the propagation of the flame (Mallard and Le Chatelier, 1883). Further theories, such as

the Semenov theory, included the effects of the diffusion of molecules in the propagation

of the flame wave, but did not include radical diffusion (Glassman and Yetter, 2008).

Eventually, the theories of laminar flame propagation came to include radical diffusion.

In 1947, Tanford and Pease theorized that it was radical diffusion from the reaction zone

back to the reactants that controlled the flame propagation. It is now known that it is the

diffusion of heat and mass from the reaction zone to the unburned reactants that causes

the propagation of laminar premixed flames (Glassman and Yetter, 2008). While

underlying mechanism assumed by Mallard and Le Chatelier proved to be only partially

correct, their work did produce two order of magnitude approximations that are important

to this day (Glassman and Yetter, 2008). They are given in Equations 1-4 and 1-5.

$$\delta_L \sim \frac{\alpha}{S_L} \tag{1-4}$$

$$S_L \sim (\alpha RR)^{1/2} \tag{1-5}$$

where δ_L is the thickness of the flame wave, α is the thermal diffusivity of the unburned

gas, and RR is the overall reaction rate of the combustion. Equation 1-4 basically states

that for similar fuel-air mixtures, the flame thickness will varying inversely to the laminar

flame speed. The implication of Equation 1-5 is that the laminar flame speeds varies with

the overall reaction rate of the combustion process. Fuels that react faster will have

higher laminar flame speeds and thus thinner flame thicknesses. Equations 1-4 and 1-5

also show that the thermal diffusivity of the unburned mixture is important in

determining the laminar flame speed and the flame wave thickness.

1.1.4 Biomass Derived Fuels

One alternative fuel source that is sustainable in nature is the production of fuels

from biomass. Fuels produced from biomass vary in composition depending on the

biomass source and the process used to convert the biomass to fuel. Two common

biomass derived fuels are landfill gas and synthesis gas, or syngas. Landfill gas is

produced by bacterial decomposition of organic waste, such as that typically contained in a landfill (Bade et al., 2008). The composition of landfill gas varies based on the conditions present at a particular landfill. In general, landfill gas is comprised of around 50% methane and 50% carbon dioxide, on a molecular basis. It is common practice to "flare" landfill gas. That is, the gas is burnt without any real use to prevent it from venting to the atmosphere (Bade et al., 2008). This makes landfill gas an attractive option as a fuel due to its relative abundance and the fact that it is not currently being utilized. One particular variety of landfill gas that has been studied is composed of 55% methane and 45% carbon dioxide, on a molecular basis (Liu et al., 2010a). This variety of landfill gas is studied in this thesis and is henceforth referred to as *LG*.

Syngas is a mixture of hydrogen and carbon monoxide that can be produced from any number of gaseous, liquid, or solid fuels. There are many processes that are used to convert fuel sources into syngas, including steam reforming, partial oxidation, and autothermal reforming (Liu et al., 2010b). The molecular ratio of hydrogen and carbon monoxide in the syngas depends on the chemical makeup of the fuel it is derived from and on the process that is used to produce the syngas. For instance, steam reformation of methane results in a syngas blend of 25% carbon monoxide and 75% hydrogen while partial oxidation of methane results in a syngas blend of 33% carbon monoxide and 67% hydrogen (Liu et al., 2010b). For fuels with a higher carbon to hydrogen content, such as biomass and coal, the syngas mixture can have higher amounts of carbon monoxide than hydrogen. Two syngas blends that have been studied as biomass derivatives are a blend of 5% hydrogen and 95% carbon monoxide, referred to as *SG05*, and a blend of 50% hydrogen and 50% carbon monoxide, referred to as *SG50* (Liu et al., 2010a; McLean et al., 1994). These two blends of syngas are studied in this work.

1.1.5 Carbon Dioxide Capture through Oxyburn

There are multiple techniques used to capture the carbon dioxide produced by the combustion of hydrocarbon fuels. The main difficulty in sequestering carbon dioxide is the presence of nitrogen in air. Stoichiometric combustion of hydrocarbons with air will result in the products carbon dioxide, water, and nitrogen. Water can be readily removed from the products via condensation by taking advantage of the relatively high boiling temperature of water. However, separating the carbon dioxide and nitrogen requires a process such as monoethanolamine (MEA) chemical absorption and is an energy intensive process (Ho et al., 2006; Dudgeon, 2009). Another strategy for capturing carbon dioxide from a combustion process is to combust the fuel with pure oxygen. If this is done at stoichiometric conditions, the products of combustion are almost exclusively carbon dioxide and water, which can be easily separated. This technique requires the separation of oxygen from the nitrogen in air upstream of the combustion process through a technique such as pressure swing adsorption (Kearns and Webley, 2006). Since the separation of oxygen from nitrogen requires energy, it follows that the combustion should be carried out at stoichiometric conditions to fully use all the oxygen. This also simplifies the carbon dioxide separation process in the products. One possible drawback to this scenario is that combustion of hydrocarbons with pure oxygen results in temperatures nearly 1000 K higher than combustion with air, as described previously. These high temperatures can create problems with the materials in combustion devices, which are not designed to handle such extreme temperatures. A proposed solution to the issue is to recirculate carbon dioxide back from the combustion products and blend it with oxygen. This results in lower flame temperatures while still allowing carbon dioxide to be captured since the products of reaction will still be water and carbon dioxide. For this reason, combustion with an oxidizer consisting of oxygen and carbon dioxide is studied in this thesis.

1.2 Specific Objectives

The specific objectives for this work are (a) to develop a working computational model to study the combustion process of two-dimensional laminar premixed flames with detailed chemical kinetics, (b) to apply this model to biomass derived fuels to compare their combustion properties with methane, and (c) to apply this model to study a proposed technique of combustion with an oxidizer consisting of carbon dioxide and oxygen for the purposes of carbon dioxide capture and sequestration.

CHAPTER 2: THEORETICAL CONSIDERATIONS

2.1 Chemical Kinetics

At the heart of the work presented here is the coupling of two fields of study: chemical kinetics and fluid dynamics. The theory governing chemical kinetics is presented first. Chemical kinetics governs the behavior of reacting chemical species. As explained earlier, a combustion reaction proceeds over many reaction steps, characterized by the production and consumption of intermediate reactants. Several conditions determine the rate at which reactions take place. Perhaps the important conditions determining the rate of reaction are the concentration of reactants and the temperature (Glassman and Yetter, 2008). The concentration of the reactants affects the probability of a reactant collision, while the temperature determines the probability of the reaction occurring given a collision.

In general, a chemical reaction can be written in the form

$$\sum_{i=1}^{N_r} v_i' \chi_i \leftrightarrow \sum_{i=1}^{N_p} v_i'' \chi_i \tag{2-1}$$

where N_r is the number of reactant species, N_p is the number of product species, v_i' is the stoichiometric coefficient of reactant species i, v_i'' is the stoichiometric coefficient of product species i, and χ_i is the chemical symbol for the ith species (Glassman and Yetter, 2008).

The net rate of production for each species i as a result of reaction k is denoted as $w_{i,k}$. The rate of production can be defined as

$$w_{i,k} = \left(\frac{d[\chi_i]}{dt} \right)_k = \left(v_{i,k}'' - v_{i,k}' \right) \left(k_{f,k} \prod_{j=1}^{N_r} [\chi_j]^{v_{j,k}'} - k_{r,k} \prod_{j=1}^{N_p} [\chi_j]^{v_{j,k}''} \right) \tag{2-2}$$

where $[\chi_i]$ is the molar concentration of species i with chemical symbol χ, k_f is the forward rate reaction constant, k_r is the reverse rate reaction constant, and subscript k denotes terms with respect to reaction k (Glassman and Yetter, 2008; Kuo 2005).

It has been found that a way to describe the forward rate constant is the Arrhenius form

$$k_{f,k} = A_k \exp\left(-\frac{E_k}{RT}\right) \tag{2-3}$$

where E is the activation energy of the reaction, R is the universal gas constant, A is the pre-exponential factor, T is the temperature, and subscript k denotes terms with respect to reaction k. The pre-exponential factor takes into account the factors affecting collision frequency other than species concentrations (Glassman and Yetter, 2008).

However, Equation 2-3 does not take into account the temperature dependence of the pre-exponential term. A standard form to take this property into account is the modified Arrhenius form

$$k_{f,k} = A_k T^{\beta_k} \exp\left(-\frac{E_k}{RT}\right) \tag{2-4}$$

where β_k is the temperature exponent of the reaction (Glassman and Yetter, 2008). In general, the values A_k, β_k, and E_k are properties of the reaction that are determined experimentally. Essentially, Equations 2-3 and 2-4 state that the rate of reaction generally increases as the temperature increases.

For most reactions, the reverse rate constant can then be computed from the forward rate constant using

$$k_{r,k} = \frac{k_{f,k}}{K_k} \tag{2-5}$$

where K_k is the equilibrium constant of the *k-th* reaction (Glassman and Yetter, 2008). For certain reactions, especially slow ones, Equation 2-5 does not apply, so the backward rate constant has to be specified (Glassman and Yetter, 2008).

The aforementioned expressions can then be applied to every species and reaction present in order to determine the overall rate of production or consumption of each species.

2.2 Chemical Kinetic Mechanisms

2.2.1 Kinetic Mechanisms Overview

In order to describe all the reactions present in a complex reaction event such as combustion, a kinetic mechanism can be developed. A kinetic mechanism contains a compilation of all the species, reactions, and reaction rate parameters involved in a particular reaction process.

In the field of hydrocarbon combustion, chemical kinetic mechanisms can range in their completeness describing the breadth of the reactions and species involved. In a way, there are two different categories of mechanisms: reduced and comprehensive. Comprehensive mechanisms attempt to completely describe the overall reaction mechanism by including all possible species and reactions. Reduced mechanisms attempt to describe the reaction process while striking a balance between accuracy and computational expense. There are many examples of reduced kinetic mechanisms for hydrocarbon combustion, e.g. Bilger et al. (1989).

Comprehensive mechanisms have been developed for both simple and complex hydrocarbons (Curan et al., 2002; Smith et al., 2010). The computational expense of such comprehensive models can be significant. This is especially true for complex hydrocarbon models such as the one in Curan, et al. (2002). These models can contain hundreds of species and thousands of reactions.

In the work presented here, only reactions involving fuels with a single carbon atom or less were studied. This includes methane, carbon monoxide, and hydrogen. Perhaps the most popular "single carbon" hydrocarbon reaction mechanism today is the Gas Research Institute (GRI) mechanism (Smith et al., 2010; Bowman et al., 1995). This mechanism was designed to model natural gas combustion. Since the GRI mechanism describes the combustion of methane, it also must include the combustion mechanisms for other fuels that are included in the kinetics mechanism, such as CO and H_2

(Westbrook and Dryer, 1981). In the case of the GRI mechanism, the size of the comprehensive model is more manageable by today's computers. However, there still are limitations on computer software that pose issues. The most complete and accurate version of the GRI mechanism is version 3.0, which contains 325 reactions and 53 species (Smith et al., 2010). Unfortunately, the computational fluid dynamics software used in this work, FLUENT, only allowed a maximum of 500 reactions and 50 species, precluding the use of GRI mechanism 3.0. The previous version of the GRI mechanism is version 2.11. This version of the mechanism contains 277 reactions and 49 species, allowing it to be used with FLUENT (Bowman et al., 1995). Although GRI mechanism 2.11 is not the most recent mechanism for methane kinetics, it is still an accurate mechanism that has been utilized in the research community for more than a decade with valid results, e.g. see Hawkes et al. (2004) and Pitsch and Steiner (2000). The methane kinetics model in GRI version 2.11 was used in the research for this thesis.

2.2.2 Basic Mechanism Pathways for Methane and "Wet" Carbon Monoxide Combustion

Although it would be tedious to list the entire GRI kinetic mechanism, it is useful to examine the basic kinetic reaction routes for the oxidation of the fuels studied in this research. This helps validate results and develop a better understanding of the overall combustion process.

As was mentioned earlier, this work studies fuels comprised of CH_4, CO, and H_2 as the reactive species. The basic methane oxidation reaction mechanism is presented first. Methane is unique from most other hydrocarbon fuels in that it is extremely stable against oxygen attack at low temperatures. This results in two different reaction mechanisms, a low temperature mechanism and a high temperature mechanism (Glassman and Yetter, 2008). The major steps for high temperature mechanism of methane can be described by the following nine reactions (Glassman and Yetter, 2008)

$$CH_4 + M \rightarrow CH_3 + H + M \tag{2-6}$$

$$CH_4 + X \rightarrow CH_3 + XH \tag{2-7}$$

$$CH_3 + O_2 \rightarrow CH_3O + O \tag{2-8}$$

$$CH_3 + O_2 \rightarrow H_2CO + OH \tag{2-9}$$

$$CH_3O + M \rightarrow H_2CO + H + M \tag{2-10}$$

$$H_2CO + X \rightarrow HCO + XH \tag{2-11}$$

$$HCO + M \rightarrow H + CO + M \tag{2-12}$$

$$CH_3 + CH_3 \rightarrow C_2H_6 \tag{2-13}$$

$$CO + OH \rightarrow CO_2 + H \tag{2-14}$$
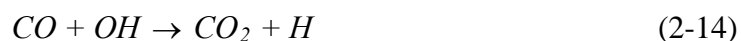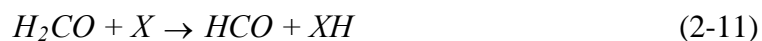
where M is any available third body species and X is any of the available radicals, such as OH, O, H, and HO_2 (Glassman and Yetter, 2008). Reactions 2-6 and 2-7 are the chain initiation steps which begin the breakdown of methane. Note that if OH is the radical in reaction 2-7 or 2-11, H_2O is produced. This is the case later in the reaction zone, as OH concentrations begin to increase due to dissociation reactions at higher temperatures. Reactions 2-8, 2-9, 2-10, 2-11, and 2-12 all add radicals to the reaction pool and lead to the production of CO (Glassman and Yetter, 2008). Reaction 2-13 represents the recombination of methyl radicals into ethane. This can result in a significant amount of ethane being formed in the system (Warnatz, 1981), so ethane oxidation must be included in a full methane reaction mechanism. When OH is the radical, which is often the case, Reaction 2-14 is relatively slow compared to Reaction 2-7. This results in CO building up early in methane oxidation, and then being consumed later when CO and OH concentrations are sufficiently high (Glassman and Yetter, 2008). The consumption of CO results in the major heat release in the overall reacting system (Glassman and Yetter, 2008). It is important to note that there are numerous other reactions that contribute to the combustion of methane that are not mentioned above. However, these additional reactions are included in the full methane mechanism used in this work.

The other basic reaction mechanism presented in this work is the oxidation of "wet" CO. The term "wet" when used to describe CO oxidation refers to the presence of hydrogen containing molecules in the reacting medium. It has been found that the reaction mechanism of CO varies significantly in the presence of the hydrogen containing molecules (Brokaw, 1967). For the work in this thesis, the oxidation of CO always occurs alongside a hydrogen containing species, specifically H_2. With this in mind only the wet combustion of CO is presented here. The major reactions governing the wet combustion of CO in the presence of H_2 are (Glassman and Yetter, 2008)

$$CO + O_2 \rightarrow CO_2 + O \tag{2-15}$$

$$H + O_2 + M \rightarrow HO_2 + M \tag{2-16}$$

$$O + H_2 \rightarrow OH + H \tag{2-17}$$

$$OH + H_2 \rightarrow H_2O + H \tag{2-18}$$

$$O + H_2O \rightarrow 2OH \tag{2-19}$$

$$CO + OH \rightarrow CO_2 + H \tag{2-20}$$

$$H + O_2 \rightarrow OH + O \tag{2-21}$$

The reaction mechanism for H_2 oxidation becomes important in the process described above and is reviewed in greater detail in Glassman and Yetter (2008). As can be seen in Reactions 2-15 through 2-21, the mechanism starts with the chain initiating step in Reaction 2-15. The O radicals produced in this step then are used in Reactions 2-17 and 2-19. Reactions 2-17 and 2-19 are chain branching steps that increase the radical pool. At lower temperature, Reaction 2-16 leads to the creation of hydrogen peroxide, H_2O_2, which eventually dissociates into OH radicals at high temperatures. As explained earlier, Reaction 2-20 proceeds when the CO and OH concentrations allow for it (Glassman and Yetter, 2008).

2.3 Fluid Dynamics

As alluded to earlier, the work presented in this study is based on the coupling of chemical kinetics and fluid dynamics. The fundamental theory governing fluid dynamics is presented in this section.

The study of fluid dynamics breaks down into three basic principles: the conservation of mass, Newton's second law of motion, and the conservation of energy. However, the complexity of fluid dynamics is significantly greater than those simple principles make it appear. The work presented in this paper was conducted at steady state without the presence of gravitational effects. With that in mind, all the fluid dynamics equations presented here already take these factors into account. Assuming steady state, the conservation of mass can be described in the following partial differential equation (Anderson, 1995)

$$\nabla \cdot \left(\rho \, \vec{v} \right) = 0 \tag{2-22}$$

where ∇ is the del operator, ρ is density and $\vec{v}$ is the velocity vector. Equation 2-22 is basically stating that the summation of mass through the surfaces of a fluid element must equal zero. In other words, no mass is being created or destroyed.

For chemically reactive flow, the principle of mass conservation can be applied to each individual species in the form of species conservation. There are a couple of differences between species conservation and mass conservation. In species conservation, species diffusion must be taken into account. In fact, species diffusion is fundamentally important in the propagation velocity of laminar premixed flames, as implied by Equation 1-5 (Glassman and Yetter, 2008). Additionally, individual chemical species can be created or destroyed due to chemical reactions, as described in Equation 2-2. In general, the conservation of each species i in a reacting flow can be described by (Yeoh and Yuen, 2009; FLUENT, 2009)

$$\nabla \cdot \left(\rho \vec{v} Y_i \right) = -\nabla \cdot \vec{J}_i + w_i \tag{2-23}$$

where w_i is the rate of production of species i from all chemical reactions in the system, Y_i is the mass fraction of species i, and $\vec{J}_i$ is the diffusive flux of species i. Using Fick's law, also known as the dilute approximation, and taking into account thermal effects, the diffusive flux term can be written as (FLUENT, 2009)

$$\vec{J}_i = \rho D_{m,i} \nabla Y_i - D_{T,i} \frac{\nabla T}{T} \qquad (2\text{-}24)$$

where $D_{m,i}$ is the mass diffusion coefficient for species i and $D_{T,i}$ is the thermal diffusion coefficient for species i. In physical terms, Equation 2-23 states that the net flux of a chemical species through the surface of a fluid volume is equal to the sum of the species diffusion through the surface and the species production rates from chemical reactions within the fluid volume.

Newton's second law of motion, when applied to fluid dynamics, often is referred to as conservation of momentum. Newton's second law of motion is often described by the equation *F=ma* with *F* representing force, *m* representing mass, and *a* symbolizing acceleration. When this law is applied to a fluid element, the following differential equation is derived (Anderson, 1995; FLUENT, 2009)

$$\nabla \cdot (\rho \vec{v} \vec{v}) = -\nabla p + \nabla \cdot (\bar{\tau}) + \vec{F} \qquad (2\text{-}25)$$

where *p* is the static pressure, $\bar{\tau}$ is the stress tensor, and $\vec{F}$ represents body forces. For Newtonian fluids, in which shear stress is proportional to the velocity gradient, the stress tensor is defined by (Anderson, 1995; FLUENT, 2009)

$$\bar{\tau} = \mu \left[\nabla \vec{v} - \frac{2}{3} \nabla \cdot \vec{v} I \right] \qquad (2\text{-}26)$$

where μ is the molecular viscosity and *I* is the unit tensor. To tie back into the basic form of Newton's second law, the left side of Equation 2-25 represents the momentum change, while the right side represents the sum of all the forces acting on the fluid.

The final principle governing fluid dynamics is the conservation of energy, also known as the first law of thermodynamics. In physical terms, the first law of

thermodynamics states that the rate of energy change inside a fluid element is equal to the heat flux into the element plus the work done onto the element. In mathematical terms, this can be written as (Anderson, 1995; FLUENT, 2009)

$$\nabla \cdot (\vec{v}(\rho E + p)) = \nabla \cdot \left(\lambda \nabla T - \sum_i h_i \vec{J}_i + (\bar{\tau} \cdot \vec{v}) \right) + \sum_i \frac{h_i^0}{M_i} w_i \qquad (2\text{-}27)$$

where E is the total internal energy of the fluid, λ is the thermal conductivity, h_i is the sensible enthalpy of species i at temperature T compared to a reference temperature, h_i^0 is the enthalpy of formation of species i, and M_i is the molecular weight of species i. The enthalpy of formation of a species is effectively a measure of the energy contained in the chemical bonds of the molecule.

The terms inside of the del operator on the right side of Equation 2-27 represent energy transfer due to conduction, species diffusion, and viscous dissipation, respectively. The last term on the right side of Equation 2-27 represents the energy source due to the change in enthalpy from the reactants to products in chemical reactions.

It is worth noting that Equations 2-22 through 2-27 are all partial differential equations with an arbitrary coordinate system. In the research conducted for this thesis, the coordinate system used was a two-dimensional axisymmetric variety, with radial coordinate r and axial coordinate x. Equations 2-22 through 2-27 can be expressed in axisymmetric coordinates, but the expressions are lengthy and do not offer much to this work. For expressions of these equations in axisymmetric coordinates, see Sorensen and Loc (1989) and FLUENT (2009).

CHAPTER 3: MODEL SETUP

3.1 Computational Model

To solve the governing equations of chemical kinetics and fluid dynamics, the software package FLUENT was utilized due to its ability to couple chemical kinetics and fluid dynamics. FLUENT is a computational fluid dynamics commercial software program that is used throughout the research and industrial communities. At its heart, FLUENT is a numerical solver. In computational fluid dynamics, the differential equations that govern the problem are discretized into finite volumes and then solved using algebraic approximations of differential equations. These numerical approximations of the solution are then iterated until adequate flow convergence is reached. FLUENT is also capable of importing kinetic mechanisms and solving the equations governing chemical kinetics. The chemical kinetics information is then coupled into fluid dynamics equations to allow both phenomena to be incorporated into a single problem.

Since FLUENT is a packaged software package, it comes with certain limitations. As was mentioned earlier, the current version of FLUENT is limited to kinetics mechanisms with 500 reactions and 50 chemical species. This precludes many mechanisms, such as those in Curran et al. (2002) and Smith et al. (2010).

There are many options to specify when setting up a computational fluid dynamics model. The options used in this work are presented in Table 3-1.

Table 3-1. Computational model setup.

Solver Type	Pressure Based
Viscous Model	Laminar
Gravitational Effects	Off
2D Space	Axisymmetric
Pressure-Velocity Coupling	SIMPLE
Momentum Equation Discretization	First Order Upwind
Species Equations Discretization	First Order Upwind
Energy Equation Discretization	First Order Upwind

As was explained previously, the work studied was at steady-state, so no time effects were taken into account. The viscous model was set to laminar because this work is focused only on laminar combustion phenomena. With this in mind, the Reynold's number of the unburned gases needed to be kept below 2000 to ensure laminar flow. As mentioned earlier, gravitational effects were not considered in order to eliminate unnecessary variables in analyzing the results. The physical model will be explained later, but the physical model fit appropriately with an axisymmetric coordinate system.

The SIMPLE method of velocity-coupling was used in which the mass conservation solution is used to obtain the pressure field at each flow iteration (Anderson, 1995). The numerical approximations for momentum, energy, and species transport equations were all set to first order upwind. This means that the solution approximation in each finite volume was assumed to be linear. This saved on computational expense. In order to properly justify using a first order scheme, it was necessary to show that the grid used in this work had adequate resolution to accurately capture the physics occurring within the domain. In other words, the results needed to be independent of the grid

resolution. This was verified by running simulations with higher resolution grids, as will be explained later.

In a reacting flow such as that studied in this work, there are significant time scale differences between the general flow characteristics and the chemical reactions. In order to handle the numerical difficulties that arise from this, the STIFF Chemistry Solver was enabled in FLUENT. The STIFF Chemistry Solver integrates the individual species reaction rates over a time scale that is on the same order of magnitude as the general fluid flow, alleviating some of the numerical difficulties but adding computational expense. For more information about this technique refer to FLUENT (2009).

Overall, the computational model solved the following flow equations: mass continuity, r momentum, x momentum, energy, and $n-1$ species conservation equations where n is the number of species in the reaction. The n-th species was determined by the simple fact that the summation of mass fractions in the system must equal one. Subsequently, this meant that there were 52 equations solved for each flow iteration. This does not include solving for the chemical kinetics terms that appear in the governing fluid dynamics equations.

3.2 Physical Model and Solution Procedure

3.2.1 Physical Model Description

A diagram of the physical model used in the tests for this research can be seen in Figure 3-1.
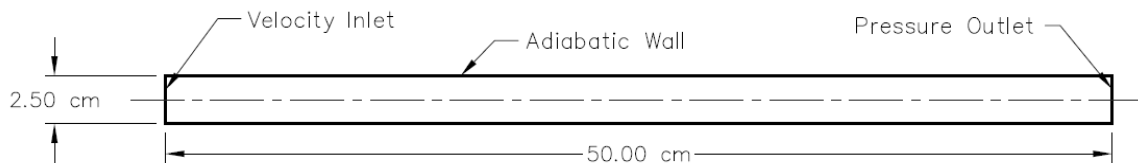
Figure 3-1. Physical model used in testing.

As can be seen in Figure 3-1, the physical model was merely a cylindrical tube with a diameter of 2.5 cm and a length of 50 cm with flow moving from left to right. The left end of the tube was set as inlet with a uniform velocity normal to the boundary. The right end of the tube was set as an atmospheric pressure outlet. The walls were set as adiabatic with zero flux of both mass and chemical species. Due to the geometry of the model, only half of the domain needed to be modeled since a symmetry condition could be assumed along the centerline of the tube.

3.2.2 Finite Volume Mesh

The physical model seen in Figure 3-1 was given a finite volume mesh to use in the computational simulations. After some trial and error, it was determined that the flame simulations were most stable with a uniform grid in the area where the flame occurred. Also, it was determined that the chemical reactions occurred within the first few centimeters of the tube. With this in mind, it was decided to employ a fine quadrangular mesh in the first seven centimeters of the tube. In this fine mesh region, the mesh was made even finer near the wall to allow for the proper processing of the boundary layer effects. The final 43 centimeters of the tube merely allowed for proper development of the combustion product flow before the atmospheric pressure outlet. This section of the model was given a relatively coarse quadrangular mesh. The size of the resulting mesh is summarized in the Table 3-2 below.

Table 3-2. Summary of simulation mesh size.

Domain Area	Number of Elements	Number of Nodes
Flame Region (First 7 cm)	38,854	43,824
Products Region (Final 47 cm)	1,920	2,057
Total Domain	40,774	45,881

As can be seen in the table above, the vast majority of the elements, more than 95%, were in the region of the domain where the reaction was to take place. This was done because this region was the area that was of interest. Within the flame region each element was approximately square with a length and width dimension of approximately 0.16 millimeters. In the boundary region, the width of each element in the r direction was about 0.08 millimeters. A view of the mesh within the flame region can be seen in Figure 3-2, with the axis at the bottom of the figure and the wall at the top.
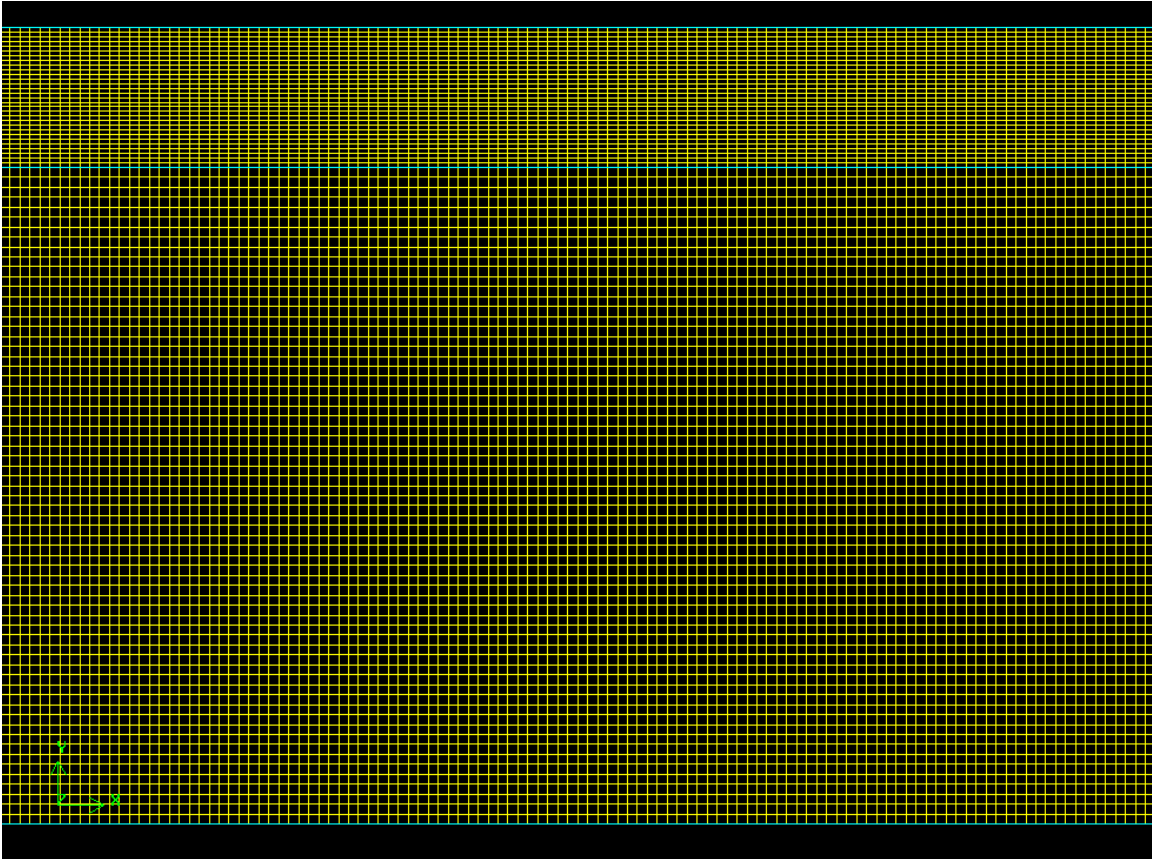
Figure 3-2. View of mesh in the flame region.

3.2.3 Solution Procedure

In order to commence a combustion process, an energy source, such as a spark, needs be added momentarily to the fuel-oxidizer mixture to commence the reaction process. This is often referred to as the activation energy of the reaction (Glassman and Yetter, 2008). This same idea holds true in the computational simulations that were performed for this thesis. Simply introducing a mixture of fuel and oxidizer would result in no substantial chemical reactions. For this reason, a "spark" zone was added less than a centimeter downstream of the inlet. The spark zone was approximately three millimeters in width and stretched across the entire cross section of the tube. The placement of the spark was inconsequential in the final shape or location of the flame that

formed. The spark simply overcomes the activation energy of the reaction and then the physics governing the problem take over to determine the final solution.

The numerical computation in this type of simulation was prone to instabilities and difficulties arriving at a converged solution. It was discovered early on that certain steps in the simulation had to be followed in a particular order to arrive at an adequate solution. Much like in cooking, the ingredients cannot be thrown together arbitrarily; they must be combined in a specific order and in a specific manner. Through trial and error, a working procedure for running the simulations was developed. The procedure was as follows:

1. A non-reacting fuel oxidizer mixture was simulated through the tube.
2. The temperature in the spark region was patched to be equal to the adiabatic flame temperature of the reaction.
3. The temperature downstream of the spark region was also set equal to the adiabatic flame temperature.
4. The species downstream of the spark region were set equal to the expected products from the overall stoichiometric reaction.
5. The reacting flow was then simulated through the tube.

In all there were 11,000 iterations for each simulation case. Step 1 above represented 1000 iterations while step 5 represented 10,000 iterations. All simulations were run in parallel on four cores of a 3.0 GHz Intel Xeon processor running Linux. The simulation time for each simulation was approximately 45 hours.

3.3 Test Conditions

As was stated previously, the purpose of this work was to utilize a computational model to study the two-dimensional combustion characteristics of methane and to compare methane with certain biofuels. In addition, the combustion properties of these fuels were studied when oxidized with an O_2/CO_2 mixture. When air was the oxidizer,

both lean and stoichiometric conditions were studied. However, when the O_2/CO_2 mixture was the oxidizer, only the stoichiometric conditions were studied for the reasoning explained in Chapter 1.

One of the first conditions that needed to be determined was the mixture ratio of the O_2/CO_2 mixture that would be used as the oxidant. As was discussed in Chapter 1, the reason the CO_2 is blended in with O_2 is to reduce the flame temperature of the reaction. With this objective in mind, a simple study was conducted on the adiabatic flame temperature of methane and *SG50* when oxidized with various mixture ratios of O_2 and CO_2. Adiabatic flame temperatures were computed using a chemical equilibrium program called CETPC. For more information about the basics of this software, see Gordon and McBride (1994). The results were plotted against the adiabatic flame temperatures of the respective fuels when oxidized with air. The results are presented in Figures 3-3 and 3-4.
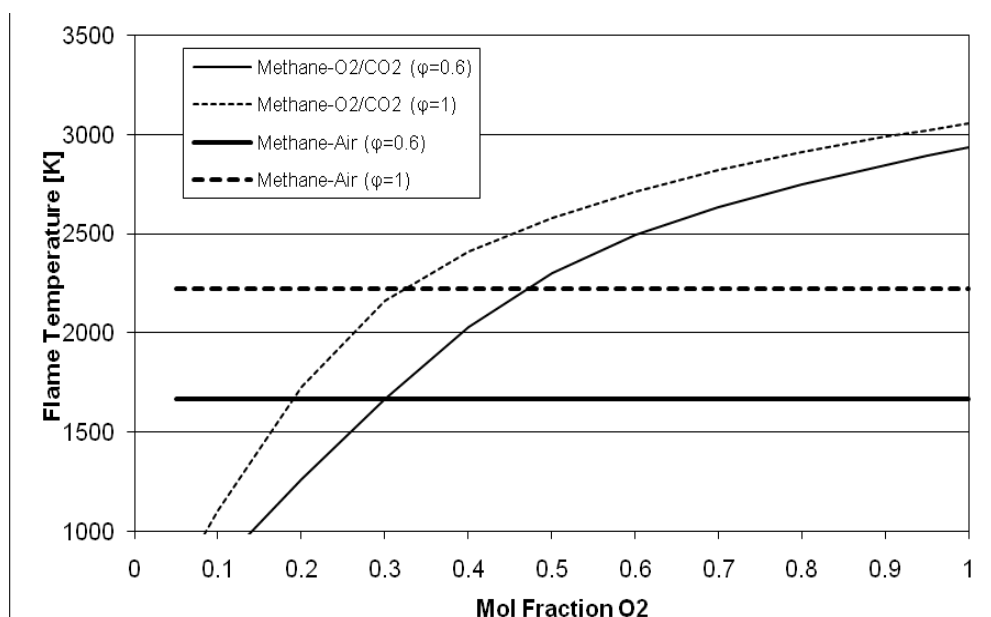

Figure 3-3. Methane adiabatic flame temperature versus mol fraction of O_2 in an O_2/CO_2 oxidizing mixture.
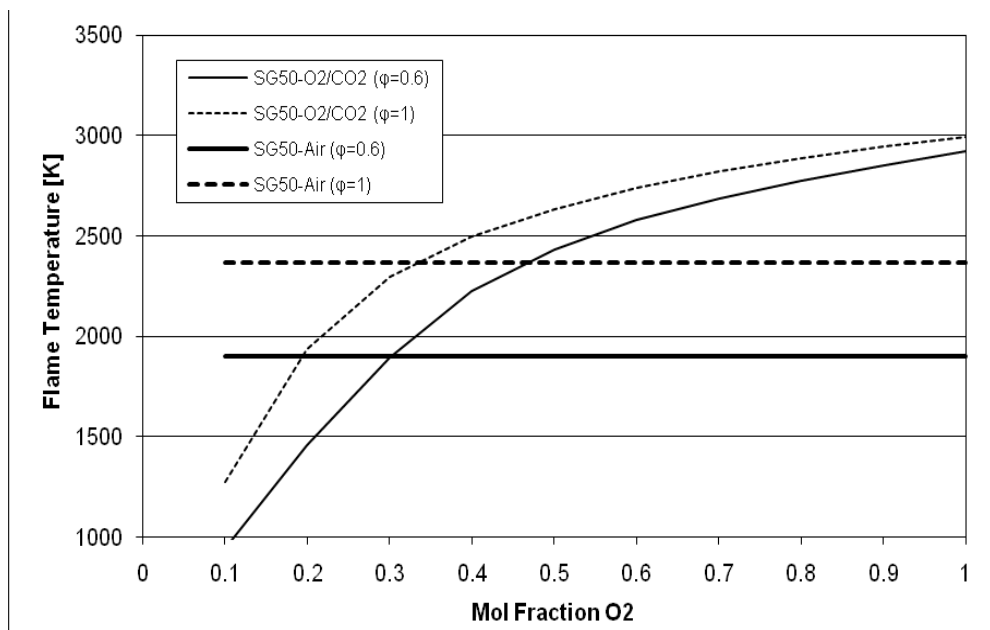
Figure 3-4. *SG50* adiabatic flame temperature versus mol fraction of O_2 in an O_2/CO_2 oxidizing mixture.

As Figures 3-3 and 3-4 show, the adiabatic flame temperature increases with increasing O_2 fraction, as is expected. The point at which the temperature of O_2/CO_2 combustion falls below the temperature of air combustion is approximately at an O_2 molecular fraction of 0.3. This appears to be mostly independent of the fuel or equivalence ratio. For this reason, the makeup of the O_2/CO_2 oxidizer was set as 30% O_2 and 70% CO_2 on a molecular basis for all cases in this study.

Methane was chosen as a fuel test case to establish the validity of the computational model. Given that methane is the major component of natural gas and is one of the simplest hydrocarbons, it has been studied extensively and was a logical choice as a baseline fuel. Methane combustion was also utilized to examine the effects that varying inlet velocities had on the flame shape and properties.

The other fuels chosen for study were landfill gas *LG* and two varieties of syngas, *SG05* and *SG50*. These fuels were chosen for multiple reasons. First off, they represent

a snapshot of the gaseous biofuels derived from biomass (Liu et al., 2010a). Also, from a more practical standpoint, they are all composed of fuel species that are contained within the chemical mechanism that was used in this work. Another reason they were chosen, again for practical purposes, was that they all had laminar burning velocities that allowed the flow to stay laminar within the physical model used in this work. Lastly, their chemical compositions allowed for some interesting analysis of chemical interactions and their effects on flame properties.

In order to determine the proper inlet velocity, denoted v_{in}, to assign to a particular case, the one-dimensional adiabatic laminar flow velocity for the fuel was used as a guideline. In general, if the inlet velocity into the tube was lower than S_L, then flashback would be expected as the flame would propagate upstream faster than the incoming fluid moved downstream (Kuo, 2005). However, if the inlet velocity was too much higher than the laminar flame speed, then the flame would essentially "blow out". The effects of flame structure near these boundary limits of v_{in} were studied for the methane case. To ensure a stable flame structure, it was found that a comfortable range at which to set v_{in} was between 50% and 100% higher than S_L for the fuel. For the simulations with the O_2/CO_2 mixture as the oxidizer, the inlet velocity was kept the same as the inlet velocity with air as the oxidizer. A summary of test conditions studied in this work is given in Table 3-3.

Table 3-3. Summary of test conditions
studied.

Fuel	Oxidizer	Φ	v_{in} [m/s]
Methane	Air	1.0	0.40
Methane	Air	1.0	0.50
Methane	Air	1.0	0.60
Methane	Air	1.0	0.70
Methane	Air	1.0	0.80
Methane	Air	1.0	1.00
Methane	Air	0.6	0.20
Methane	O_2/CO_2	1.0	0.40
LG1	Air	1.0	0.40
LG1	Air	0.6	0.15
LG1	O_2/CO_2	1.0	0.15
SG05	Air	1.0	0.70
SG05	Air	0.6	0.30
SG05	O_2/CO_2	1.0	0.70
SG50	Air	1.0	2.00
SG50	Air	0.6	0.90

As can be seen in Table 3-3, methane was studied the most in depth of all the fuels. This was because the inlet velocity of methane was varied to study its effects on the flame speed. With the exception of SG50, the biofuels were tested three different times: stoichiometric and lean conditions with air as the oxidizer, and a stoichiometric condition with O_2/CO_2 as the oxidizer.

CHAPTER 4: RESULTS AND DISCUSSION

<u>4.1 Model Verification and Fundamental Discussion</u>

In order to assure the accuracy of the results, it was first necessary to determine the validity of the computational model used in this work. The validation process involved comparisons based on thermodynamics, flame shape and structure, and flame characteristics such as S_L and δ_L. Since methane was the baseline fuel in the study, it followed that the methane-air combustion case should be used for the model validation.

In the model setup for this work, the wall was given an adiabatic condition, as seen in Figure 3-1. That means that all of the heat produced by the combustion process must be contained within the tube and moved downstream to the outlet. It becomes apparent that the temperature of the combustion products at the end of the tube should be equal to the adiabatic flame temperature of the fuel-oxidant mixture as discussed in Chapter 1. Using the chemical equilibrium program CETPC, the adiabatic flame temperature for methane was computed. At stoichiometric conditions and atmospheric pressure, the adiabatic flame temperature was estimated to be 2118 K. To compare with the results in this work, a plot of the temperature contours for a simulation of methane-air combustion is shown in Figure 4-1.
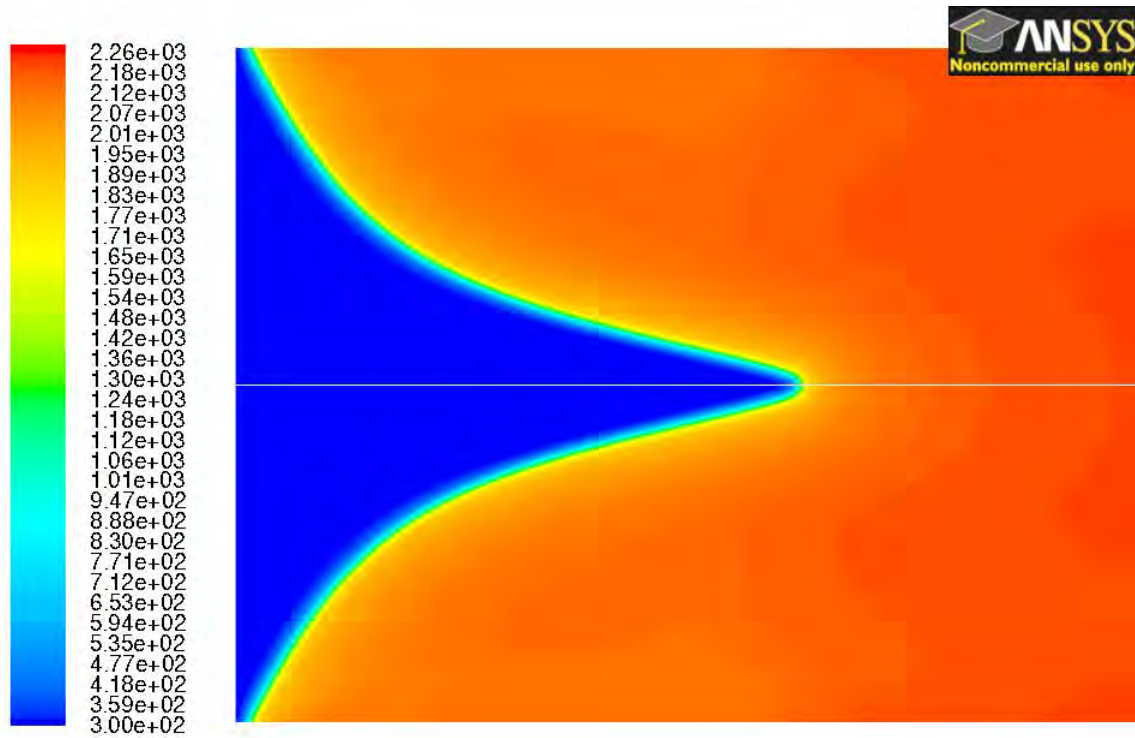
Figure 4-1. Temperature contours for methane-air combustion, ϕ =1.0, v_{in}=0.60 m/s.

By examining the scale on the left side of Figure 4-1, it is apparent that the maximum temperature seen within the simulation is on the order of 2260 K. Further analysis of the results shows that the adiabatic flame temperature predicted by the simulation was 2261 K. This is a difference of less than 7% from the value predicted by CETPC. This was deemed to be an acceptable difference when keeping in mind the different manners in which the two calculations determined adiabatic flame temperature. In addition, the adiabatic flame temperature for methane-air combustion at lean conditions (ϕ=0.6) also proved to be within range of the result predicted by the chemical equilibrium software. Since adiabatic flame temperature is only a function of the reactants and products, it follows that the adiabatic flame temperature should not change based on the inlet velocity, which proved to be the case.

Merely showing that the adiabatic flame temperature was accurate did not verify the model. It only proved that the overall thermodynamics of the reaction were proceeding as expected. The next step taken in validating the results was to compare the flame shape and structure with experimental data on premixed laminar flames. A relatively intuitive and simple way to visualize the flame is to view the temperature contours, such as in Figure 4-1. Since the reaction zone part of a flame can be defined as the region of heat release (Glassman and Yetter, 2008), it can be concluded that the temperature contours must follow the shape of the reaction zone. As a result, the region of the fluid flow with the sudden increase of temperature is approximately the area of the deflagration wave. With this in mind, it is evident that the geometry of the flame seen in Figure 4-1 is relatively conical, especially near axis of the tube. Near the walls of the tube, the flame front takes on a concave shape. This is expected as the adiabatic condition at the wall enforces the temperature gradient with respect to the radial coordinate to be equal to zero. When comparing the flame shape in Figure 4-1 with those observed in experimental work with laminar premixed flames, such as in Figure 1-3, it is easy to see the strong similarities in the geometries of the flame wave (Weinberg, 1963; Gaydon and Wolfhard, 1960). Both flames exhibit conical shapes with a slight concave shape near the outer edges of the flame. It should be noted that the physical geometries of the test apparatuses used in the referenced experiments are not identical to that used in this work. However, the setup is quite similar, so the fact that the flame shapes are so similar is valid evidence in verifying the accuracy of the results in this work.

There were three flame structure properties that were of interest in validating the model used in this work: the velocity streamlines through the flame front, S_L, and δ_L. Before any of these properties could be properly evaluated, it was first necessary to better define the limits of the flame wave. As explained in Chapter 1, a deflagration wave consists of a preheat zone and a reaction zone. The beginning of the preheat zone is often determined by the location of the first perceptible decay in the reactants (Glassman and

Yetter, 2008). This criterion was used in this work to determine the location of the beginning of the flame wave. The end of the reaction zone was more difficult to determine, as it is viewed as the location in the flame where the heat release rate of the reaction falls off sharply towards zero (Glassman and Yetter, 2008). Attempts to track the heat release rate of the reaction in FLUENT did not prove reliable, so another avenue was chosen. The major source of heat release in hydrocarbon combustion comes from the conversion of CO to CO_2, in large part due to Reaction 2-20. With this idea in mind, it stands to reason that the location where the heat release begins to drop off should coincide closely with the peak consumption of CO. Indeed, a closer look at Figure 1-5 reveals that the maximum negative slope of the CO fraction curve occurs at almost the same location as the zero intercept of the falling heat rate curve. The consumption rate of CO was a variable that could be readily tracked in FLUENT. For the sake of convenience the location of the end of the reaction zone was determined by the maximum consumption of CO within the flame for all test cases in this work.

Once the limits of the "flame wave" boundaries were properly determined, then it was possible to better study the velocity streamlines though the flame. As shown in Figures 1-2 and 1-4, the velocity streams in a laminar premixed flame proceed solely in the axial direction upstream of the flame. However, at the flame front, the streamlines expand outward to move through the flame surface in a direction that is normal to the flame front. A comparison with the work in this thesis is shown in Figure 4-2. The velocity streamlines in a methane-air combustion case are shown superimposed over the surfaces representing the beginning and end of the flame wave.
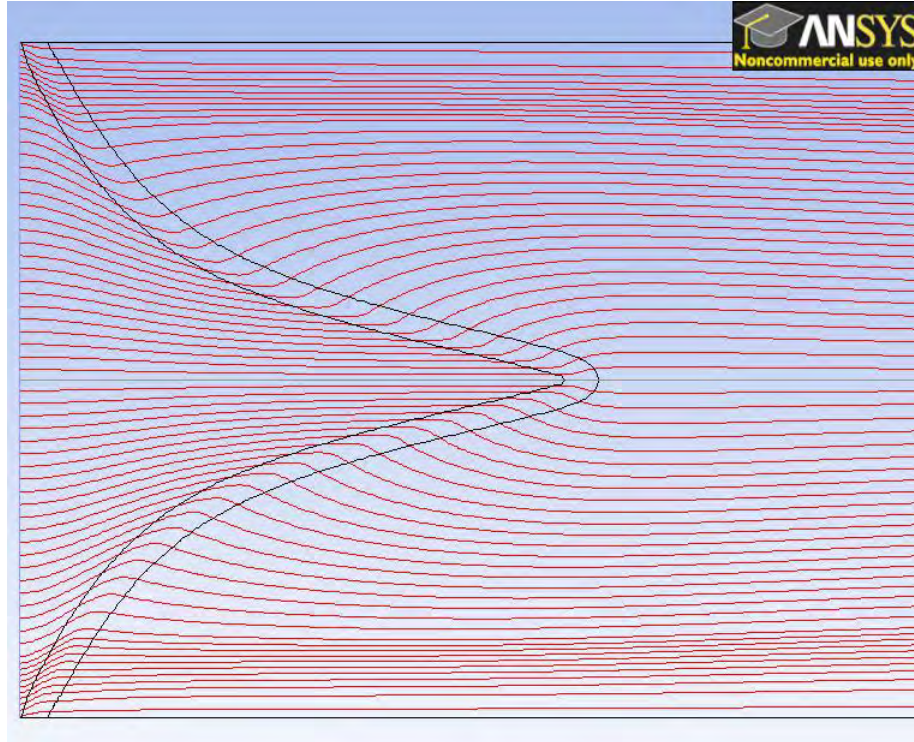
Figure 4-2. Velocity streamlines through the boundaries of a flame wave. Methane-air combustion, $\phi = 1.0$, v_{in}=0.60 m/s.

The velocity streamlines in Figure 4-2 follow a similar pattern to those observed experimentally. The flow direction is mostly in the axial direction until the flame surface, where it changes direction to move normally through the flame wave. There are only some subtle differences that can be attributed to the variations in model geometry.

The final two criteria left for validation of the model were the computed flame thickness, δ_L, and laminar flame speed, S_L, from the simulations. The thickness of a laminar flame wave is simply the distance between the beginning preheat zone and the end of the reaction zone. δ_L for stoichiometric methane-air flames has been computed numerically to be approximately 0.85 mm (Glassman and Yetter, 2008). For an inlet velocity of 0.6 m/s, the flame thickness at the wall $\delta_{L,w}$, and the flame thickness at the

axis, $\delta_{L,a}$, were computed to be 0.98 and 1.22 m/s. These fall within range of the accepted value.

The one-dimensional laminar flame speed for the stoichiometric combustion of methane and air has been measured both experimentally and numerically to be on the order of 0.38 m/s (Vagelopoulos, 1998; Liu et al., 2010a; Glassman and Yetter, 2008). Equation 1-3 was used to calculate S_L from the simulation results. The area of the flame surface, A_f, was determined to be the area of a surface midway between the boundaries of the flame wave. The surface was a contour of the mass fraction of the fuel species, since this value should represent the overall progress of the reaction. This is illustrated in Figure 4-3.
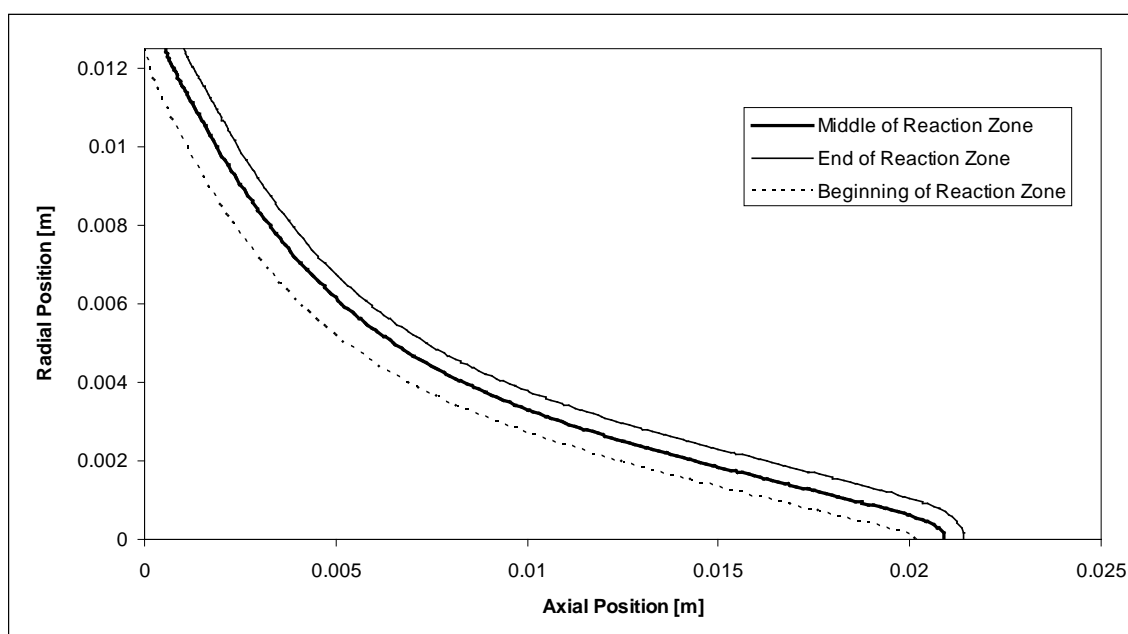
Figure 4-3. Surfaces representing the beginning, middle, and end of the flame wave. Note that the only the top have of the test domain is shown. Methane-air combustion, $\phi = 1.0$, $v_{in} = 0.60$ m/s.

At an inlet velocity of 0.6 m/s, A_f for a stoichiometric methane-air flame was determined to be 742 mm^2. Using Equation 1-3, S_L was calculated to be 0.40 m/s. This provides strong agreement with the accepted value of 0.38 m/s, with a difference of less than five percent.

As was discussed previously, a first order numerical scheme was used to solve the governing partial differential equations. In order to justify the use of this type of scheme, it was necessary to show that the results were independent of the grid resolution. Two methane-air simulations were run on grids with a finer mesh than the base grid. One grid had 36% more elements and the other had 52% more elements. Both of the grids had uniform quadrangular elements. The results from the simulations with the finer meshes showed that S_L, $\delta_{L,w}$, and $\delta_{L,a}$ varied by less than five percent from the values predicted by the base grid. This illustrated that the use of the first order numerical schemes was adequately justified.

One truth that becomes evident while analyzing the results is that the flame stabilization is dependant on the developing boundary layer near the wall. Since the inlet boundary condition is set as uniform across the entire inlet, the flow next to the wall is initially greater than zero. Indeed, the location where the flame attaches to the wall, referred to as the wall attachment point, is within a few millimeters of the inlet. It is apparent that the wall attachment point settles at the location where the velocity is slowed enough by the wall that it is equal to the laminar flame speed propagating back to the inlet. From this line of thinking, it is clear that a flame wave could not be stabilized in the manner presented here if the flow was fully developed. This is important to keep in mind if these results are being applied to practical situations. The velocity near the wall needs to be sufficiently high to support a combustion wave of this nature; hence the flow needs to still be developing.

It is clear that the methane-air combustion results compared favorably with accepted data based on thermodynamics, laminar premixed flame structure, and laminar

flame characteristics. Based on these agreements it was determined that the model was properly validated.

4.2 Methane Flame Detailed Discussion

4.2.1 Illustration of Reaction Kinetics

As a means of better understanding the physical phenomena occurring within the flame wave, it is useful to analyze the structure of the methane-air flame in more detail. The basics of the chemical kinetics occurring within a laminar premixed flame were discussed in Chapter 1 and Chapter 2. The results from this study can help illustrate that information. In all the figures in this analysis, the surfaces representing the beginning and the end of the combustion wave are plotted for reference. The propagation of the laminar flame wave is said to be dominated by the diffusion of H radicals from the reaction zone (Glassman and Yetter, 2008). Figures 4-4 and 4-5 illustrate the strong gradient in H fraction that exists across the flame wave as well as the strong thermal diffusion coefficient that exists near the end of the reaction zone. Both of these factors lead to the diffusion of H radicals against the flow and back into the preheat region.
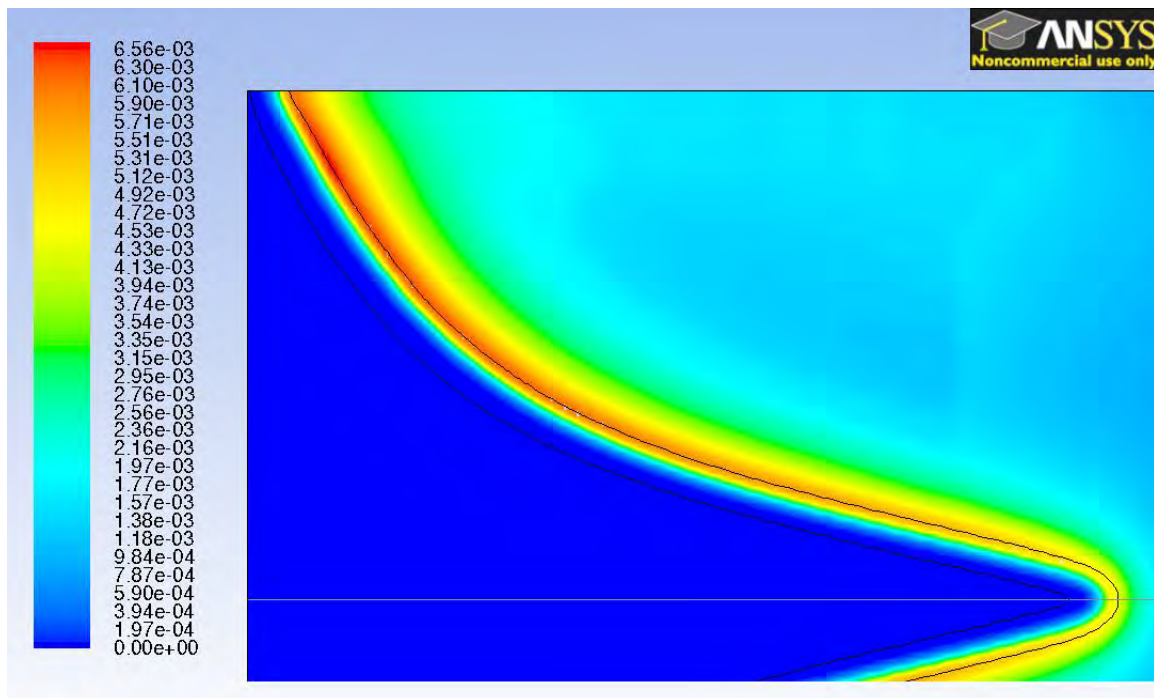
Figure 4-4. Contours of molecular fractions of *H*. Methane-air combustion, $\phi=1.0$, v_{in}=0.60 m/s.
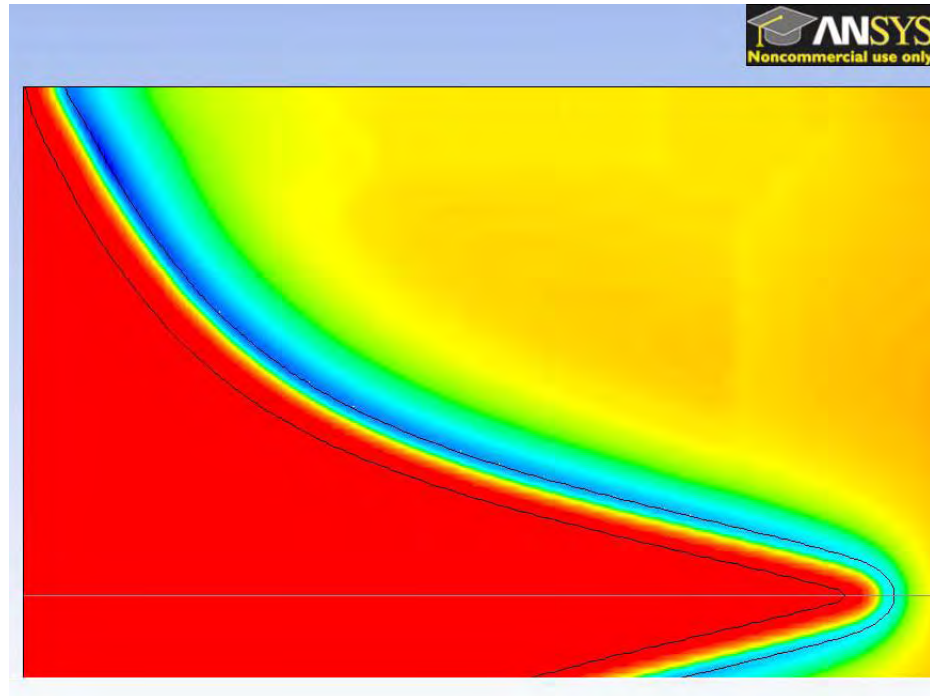
Figure 4-5. Contours of thermal diffusion coefficient of H. Note that blue contours signify the greatest negative diffusion coefficient. Methane-air combustion, ϕ=1.0, v_{in}=0.60 m/s.

Through Reaction 2-16, HO_2 begins to form in the preheat zone, as seen in Figure 4-6. At higher temperatures, the HO_2 eventually forms into OH radicals. The OH radicals become relatively abundant versus the O or H radicals in the middle to latter stages of the reaction zone, which is shown by Figure 4-7. This then leads to the decay of the fuel species and the production of H_2O through Reaction 2-7, as seen in Figures 4-8 and 4-9. Throughout the reaction zone, CO molecules build up until they are rapidly consumed by the abundant OH radicals via Reaction 2-14 (Glassman and Yetter, 2008). This is responsible for the major heat release of the combustion process and also marks the end of the reaction zone. This is illustrated in Figure 4-10.
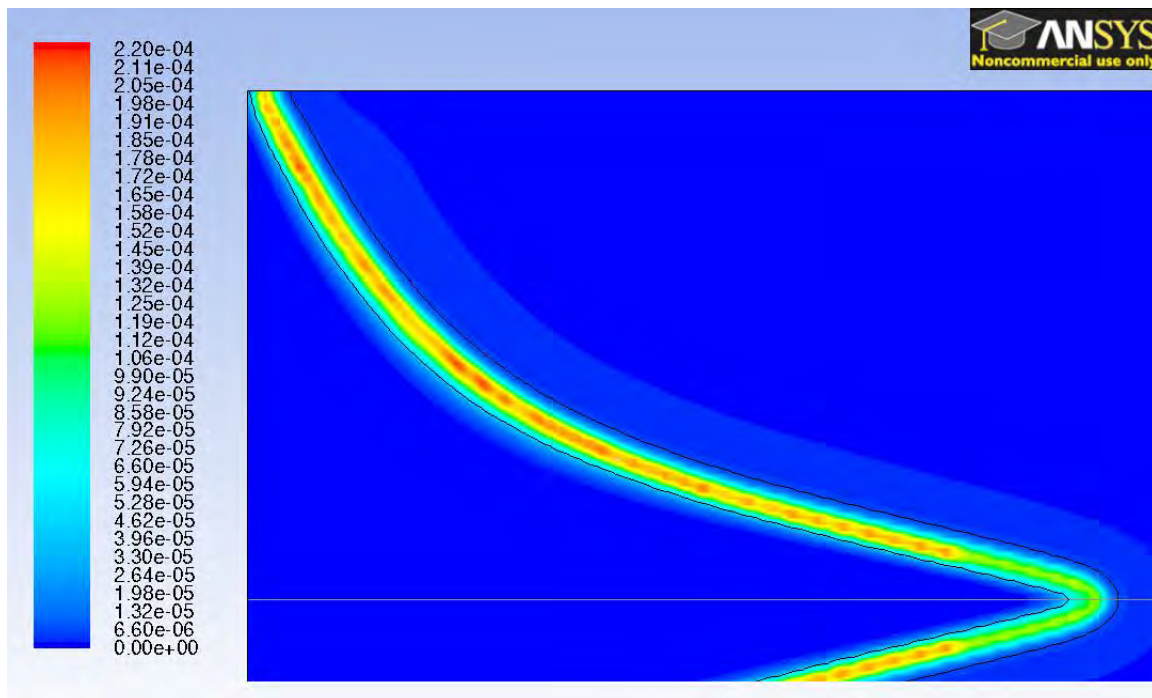
Figure 4-6. Contours of molecular fractions of HO_2. Methane-air combustion, ϕ=1.0, v_{in}=0.60 m/s.
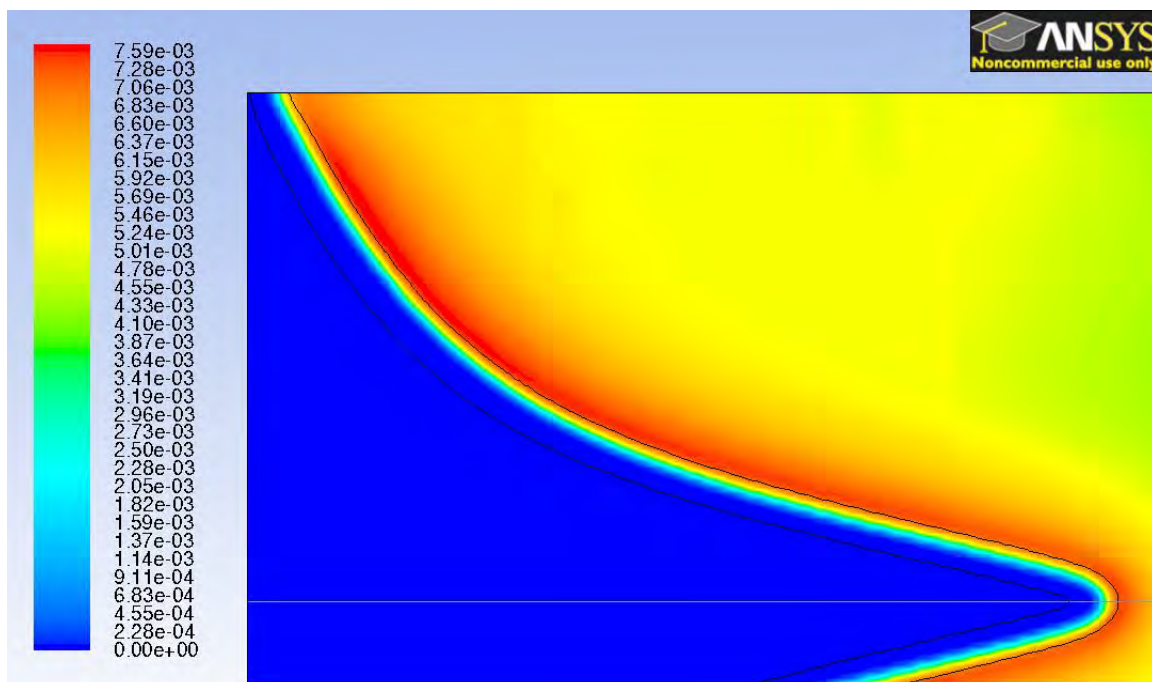
Figure 4-7. Contours of molecular fractions of *OH*. Methane-air combustion, ϕ=1.0, v_{in}=0.60 m/s.
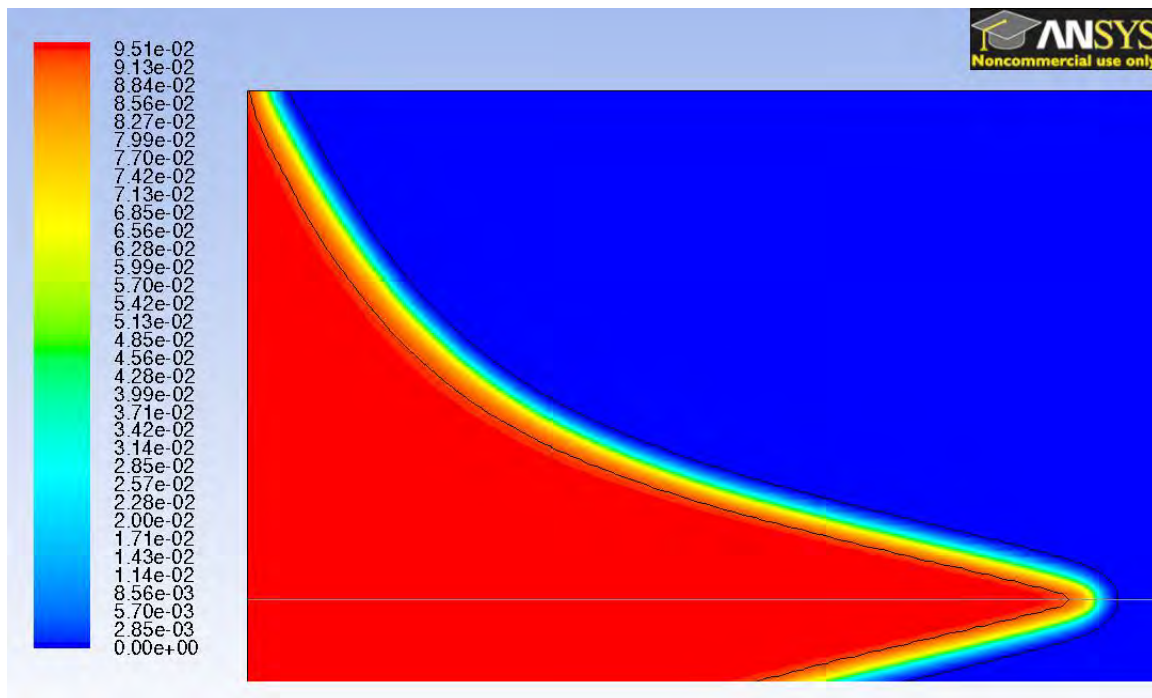
Figure 4-8. Contours of molecular fractions of CH_4. Methane-air combustion, ϕ=1.0, v_{in}=0.60 m/s.
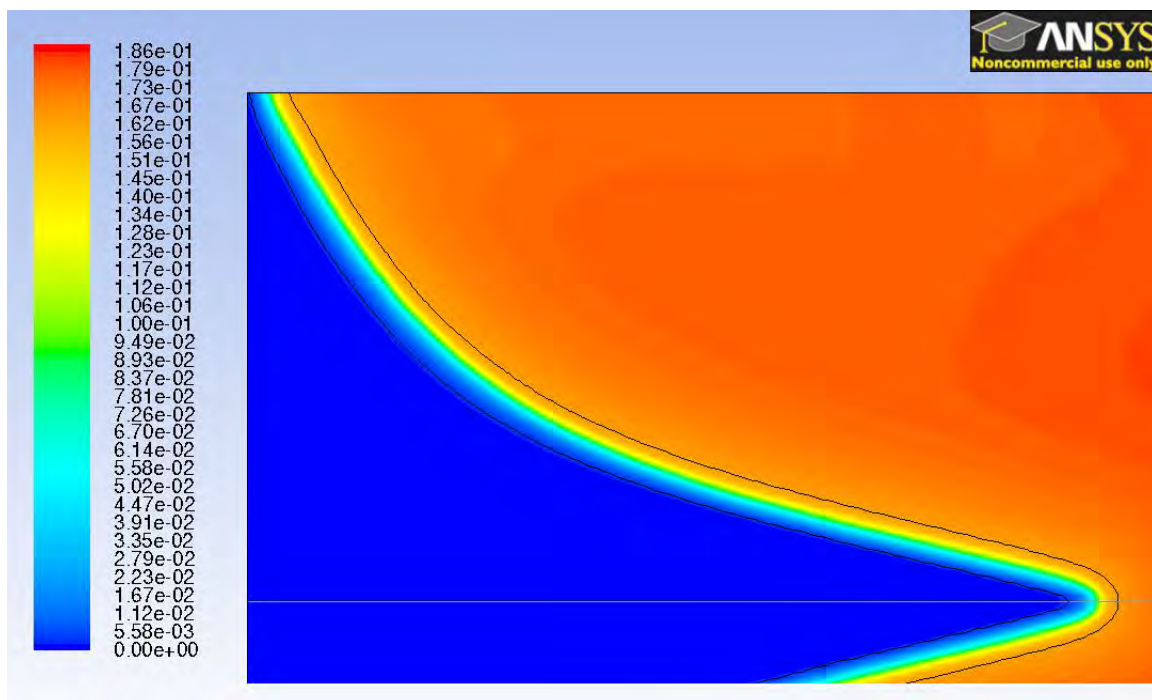
Figure 4-9. Contours of molecular fractions of H_2O. Methane-air combustion, ϕ=1.0, v_{in}=0.60 m/s.
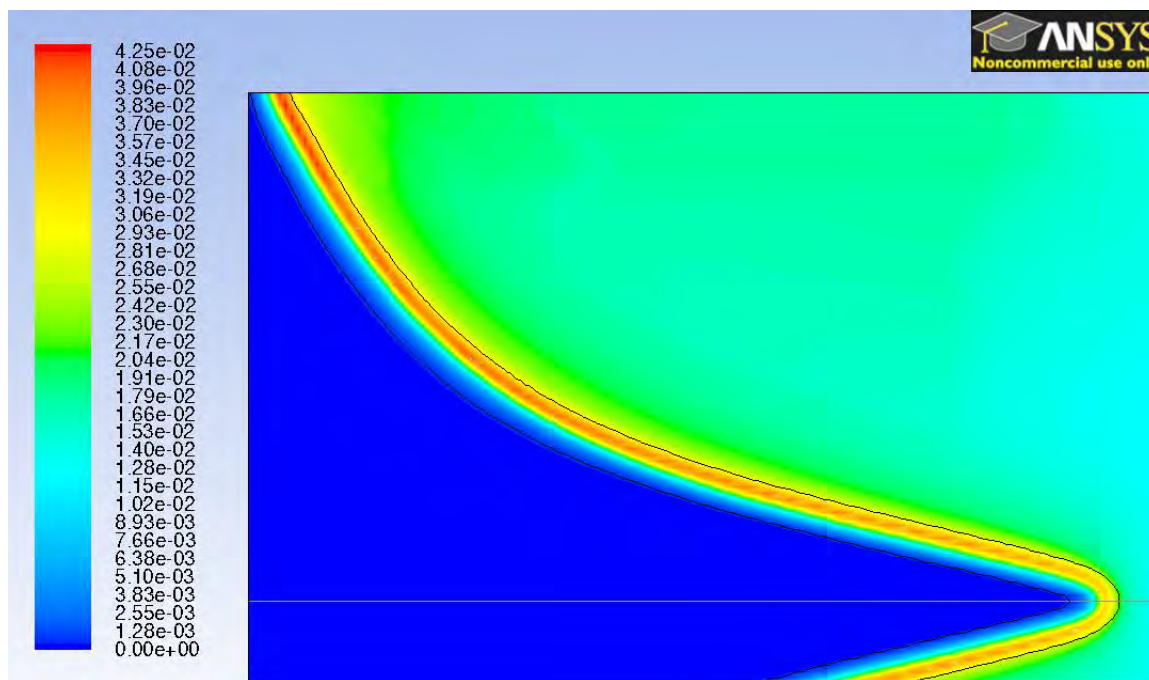
Figure 4-10. Contours of molecular fractions of CO. Methane-air combustion, ϕ=1.0, v_{in}=0.60 m/s.

It is worth noting that Figures 4-4, 4-6, 4-7, and 4-10 appear to indicate that the concentration of radicals is higher near the wall than near the centerline of the tube. However, Figures 4-1, 4-8, and 4-9 do not appear to show any disparity in the temperature or concentrations of fuel and combustion products at the axis versus at the wall. One possible explanation for this is that heat transfer allows the temperature to equalize downstream of the flame wave, preventing variations from appearing. This same explanation could apply to the fuel and products concentrations, but with species diffusion providing the means for equalizing the values downstream of the flame. However, the intermediate species occur only within the flame wave itself. Discrepancies in species concentrations that arise within the flame front are not hidden, since diffusion along the length of the flame wave does not occur as readily as diffusion throughout the entire volume of combustion products.

4.2.2 Effects of Inlet Velocity on Flame Characteristics

As Table 3-3 demonstrates, the stoichiometric methane-air simulation was run at varying inlet velocities to examine the effects of inlet velocity on the characteristics of the flame wave. Features of interest include computed values of S_L and δ_L, and the wall attachment point, defined as the location where the combustion wave makes contact with the wall. In Figures 4-11 through 4-15, the temperature contours are shown for varying inlet velocities. Refer also to Figure 4-1 for the simulation condition with v_{in} set at 0.60 m/s. These figures provide a rudimentary means of visualizing the flame waves.
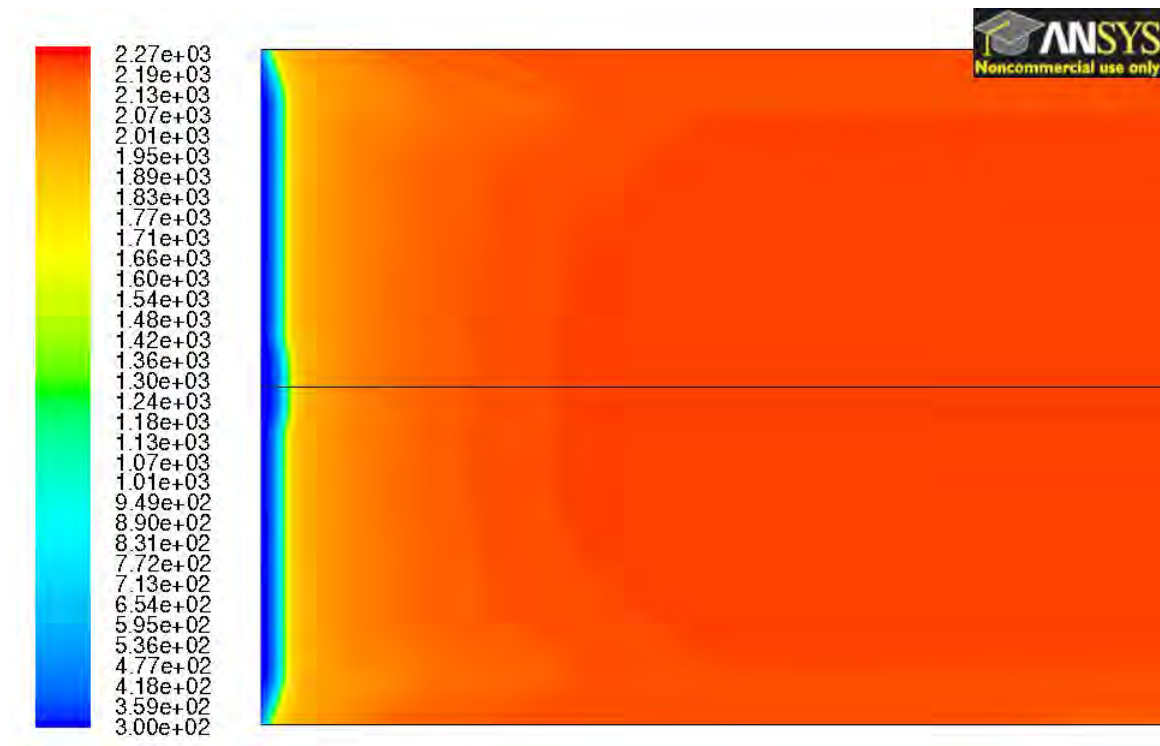

Figure 4-11. Temperature contours for methane-air combustion, ϕ=1.0, v_{in}=0.40 m/s.
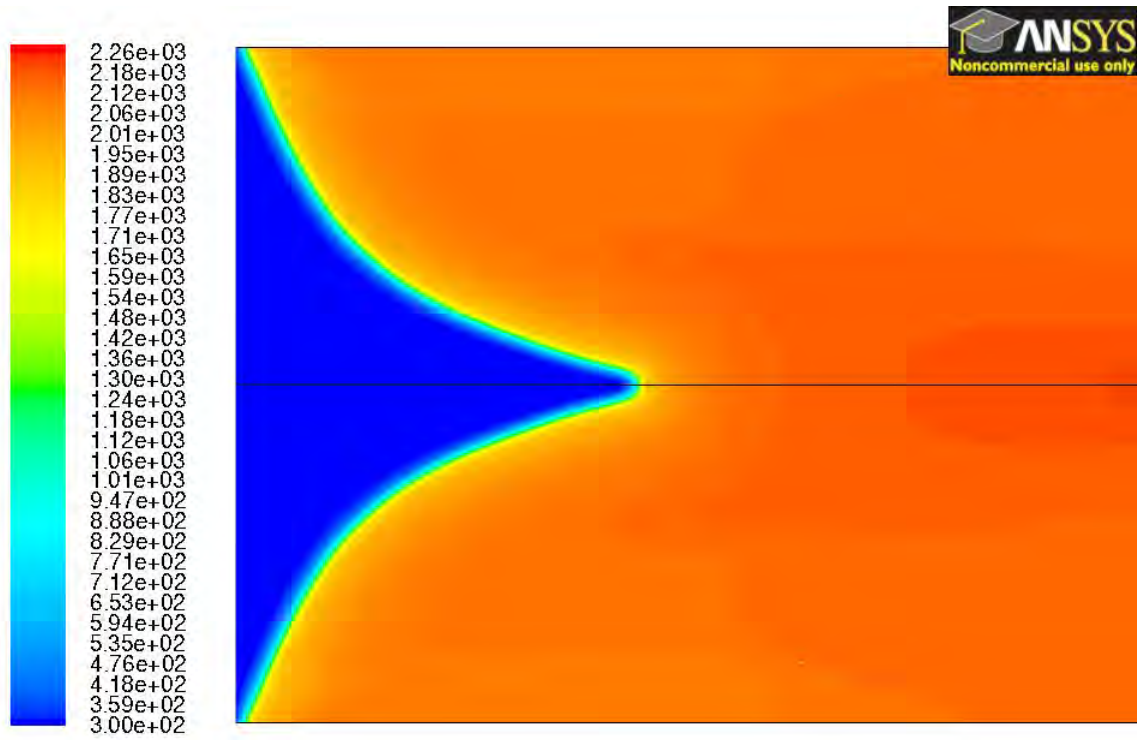
Figure 4-12. Temperature contours for methane-air combustion, $\phi=1.0$, v_{in}=0.50 m/s.
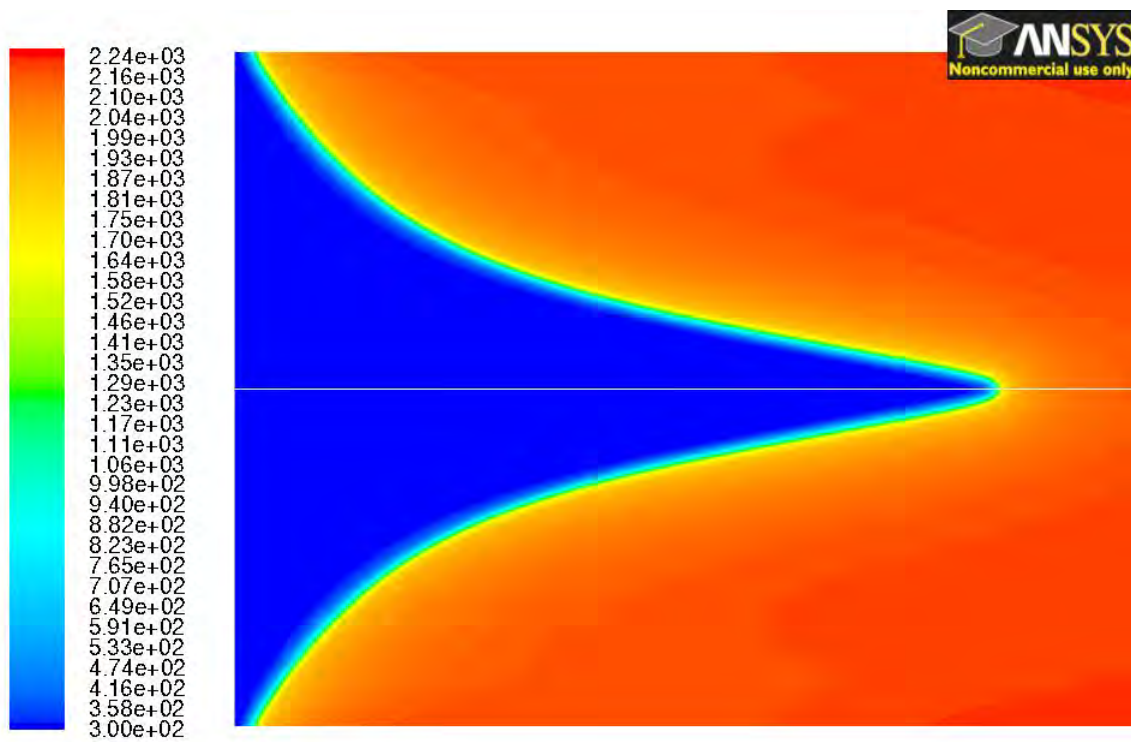
Figure 4-13. Temperature contours for methane-air combustion, $\phi = 1.0$, v_{in}=0.70 m/s.
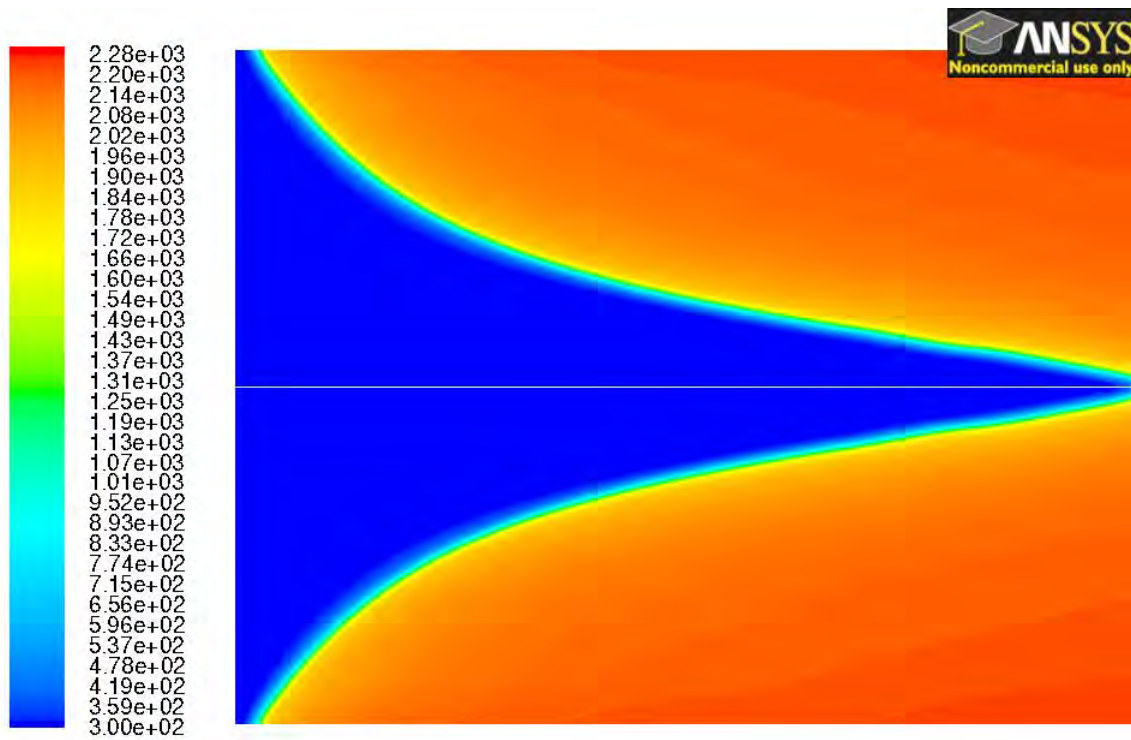
Figure 4-14. Temperature contours for methane-air combustion, ϕ =1.0, v_{in}=0.80 m/s.
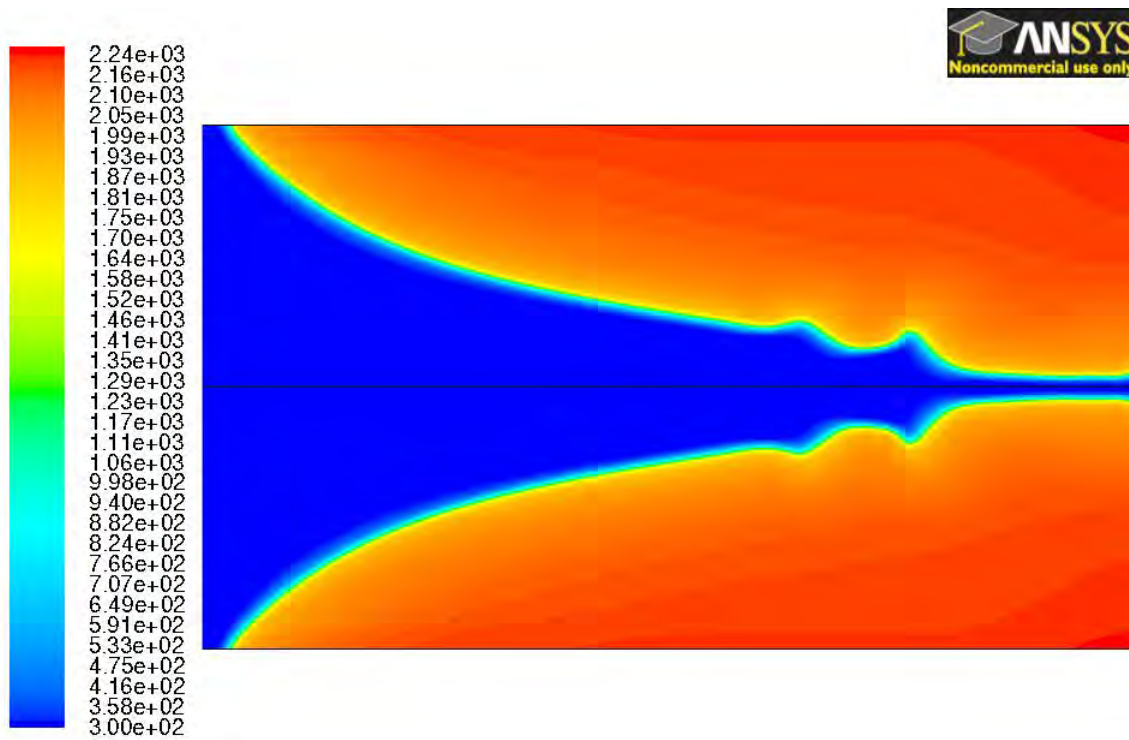
Figure 4-15. Temperature contours for methane-air combustion, ϕ =1.0, v_{in}=1.00 m/s.

It is clear from Figure 4-1 and Figures 4-11 through 4-15 that the flame wave is progressively stretched as the inlet velocity is increased above the laminar flame speed of 0.38 m/s. There comes a point when the inlet velocity is too high and the flame wave is unstable at the high velocities seen near the axis, as demonstrated in Figure 4-15. This simulation result was viewed as a nonphysical solution that would have resulted in the flame being "blown out" or developing instabilities near the axis. As such, the results from this simulation case were not analyzed.

There were five stoichiometric methane-air simulations that produced reasonable results. For each of these cases, the surface representing the center of the flame was created. Figure 4-16 shows all the flame surfaces plotted together for comparison purposes.
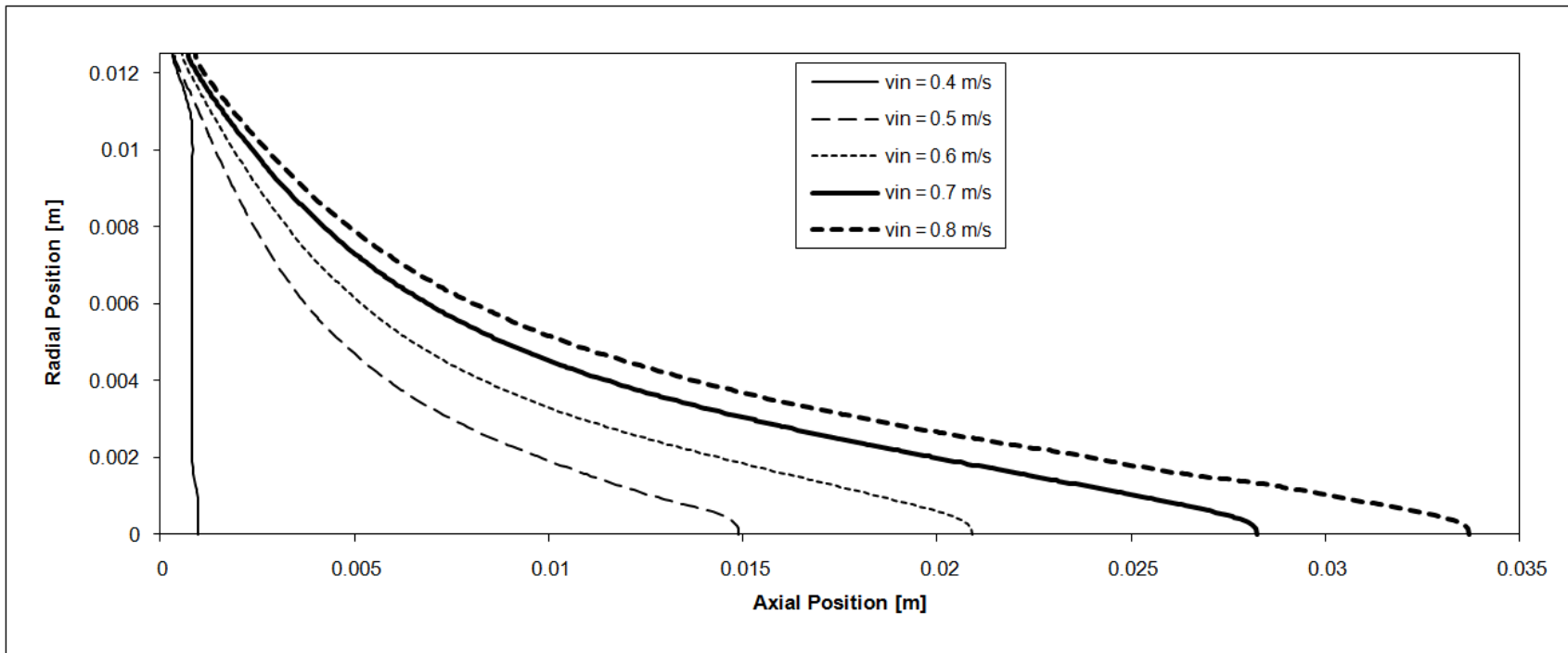
Figure 4-16. Flame surfaces for varying inlet velocities. Methane-air combustion, $\phi = 1.0$.

From analyzing Figure 4-16, a few observations stand out. First, the wall attachment point appears to move only very slightly as the velocity is increased. This makes sense considering that the wall attachment point is a result of the developing boundary layer, as described in section 4.1. Since the velocity near the wall is slowing quickly as the flow profile develops, it follows that the location of the wall attachment will not vary considerably with varying inlet velocities. In other words, small changes in axial position along the wall result in large changes in axial velocity, which in turn allows the propagating flame wave to settle at the appropriate velocity found in the range of speeds near the wall. Another observation is that there is a significant difference in the flame shape for $v_{in} = 0.40$ m/s versus $v_{in} = 0.50$ m/s. The inlet velocity at 0.40 m/s is only marginally faster than the accepted laminar flame speed. The resulting flame is mostly flat over the cross sectional area of the tube and does not exhibit a conical shape. However, at 0.50 m/s, the flame wave takes on a conical shape as the equilibrium between flame propagation and incoming fluid flow is established.

The area of the flame, A_f, and the laminar flame speed were computed for each of the different inlet velocity cases. Also, the overall flame wave thickness was determined at the axis, $\delta_{L,a}$, and wall, $\delta_{L,w}$, by computing the distance between the surfaces representing the beginning and end of the combustion wave. These results are summarized in Table 4-1.

Table 4-1. Flame characteristics for stoichiometric methane-air flames with varying inlet velocities.

v_{in} [m/s]	A_f [mm^2]	S_L [m/s]	$\delta_{L,a}$ [mm]	$\delta_{L,w}$ [mm]
0.40	496	0.40	1.05	0.87
0.50	635	0.39	1.09	0.85
0.60	742	0.40	1.22	0.98
0.70	890	0.39	1.40	1.01
0.80	1001	0.39	1.56	1.04

It is apparent from Table 4-1 that the flame characteristics $\delta_{L,a}$ and $\delta_{L,w}$ vary depending on the inlet velocity, but that S_L does not. In general, as the inlet velocity increases, $\delta_{L,a}$ and $\delta_{L,w}$ also increase. As was discussed earlier, the accepted value of S_L for one-dimensional laminar flame propagation is 0.38 m/s while the accepted flame wave thickness is 0.85 mm. All cases closely match the accepted value for S_L. When analyzing $\delta_{L,a}$ and $\delta_{L,w}$, the result that most accurately matches is the case with v_{in} set at 0.40 m/s. As the inlet velocity increases, the results for the flame wave thickness diverge further from what one-dimensional laminar flame theory predicts. This should not be a surprise considering that the flame is most one-dimensional when v_{in} is equal to 0.40 m/s, as shown in Figure 4-16.

Also, the results show that the flame wave thickness is greater at the axis than at the wall for all cases. This can be explained by the higher velocities at the axis versus the wall. At the axis the flame wave is elongated as the flow moves through the flame at a velocity higher than the one-dimensional laminar flame speed. At the wall, the flow velocity is slower and closer to the laminar flame speed, which is inherently why the flame attaches at that location. This results in a decreased flame thickness at the wall.

As was noted previously, the laminar flame speed does not appear to vary due to the changing inlet velocity. This result is interesting because it shows just how strong the principle of S_L really is. Even in a two-dimensional realm with effects from a nearby wall, the laminar flame speed remains a physical constant of the combustion process. It is clear that the phenomena that drive the flame propagation were not affected by the physical model used in this work. As can be seen in Figures 1-2 and 1-4, the path of flow through a Bunsen burner flame results in an expanding envelope of combustion gases. In the physical model utilized in this work, the tube wall prevents the formation of this expanding envelope. However, regardless of how significantly the flame is stretched, the flow field still manages to proceed through the flame in a direction nearly normal to the flame surface. Downstream of the flame, the wall effects become apparent as the

combustion gases are forced back towards the axis. This is illustrated in Figures 4-17, 4-18, and 4-19.

Figure 4-17. Velocity streamlines through the flame wave. Methane-air combustion, ϕ =1.0, v_{in}=0.50 m/s
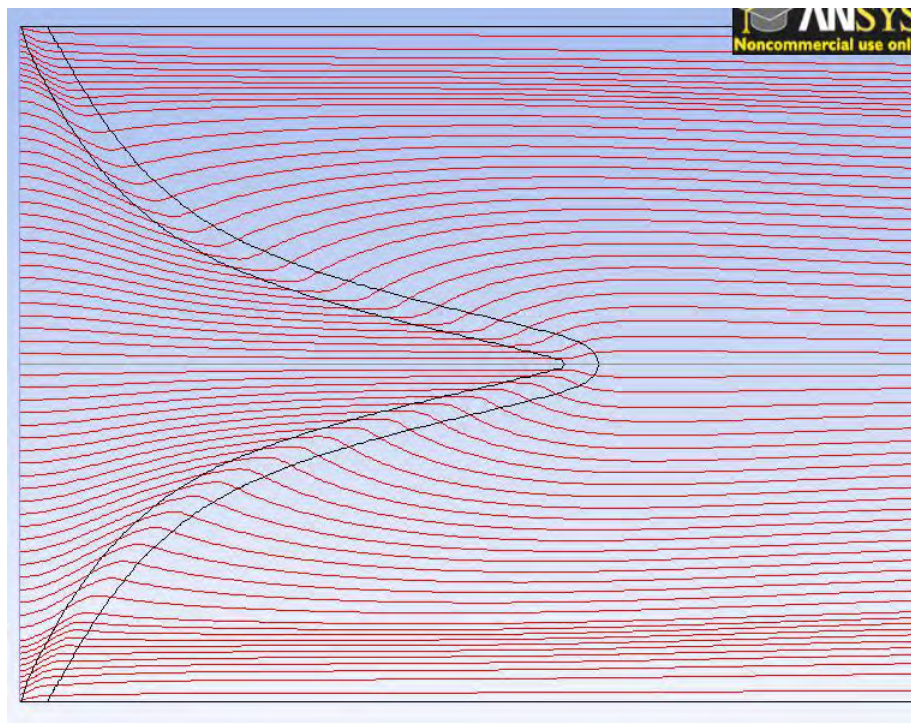
Figure 4-18. Velocity streamlines through the flame wave. Methane-air combustion,
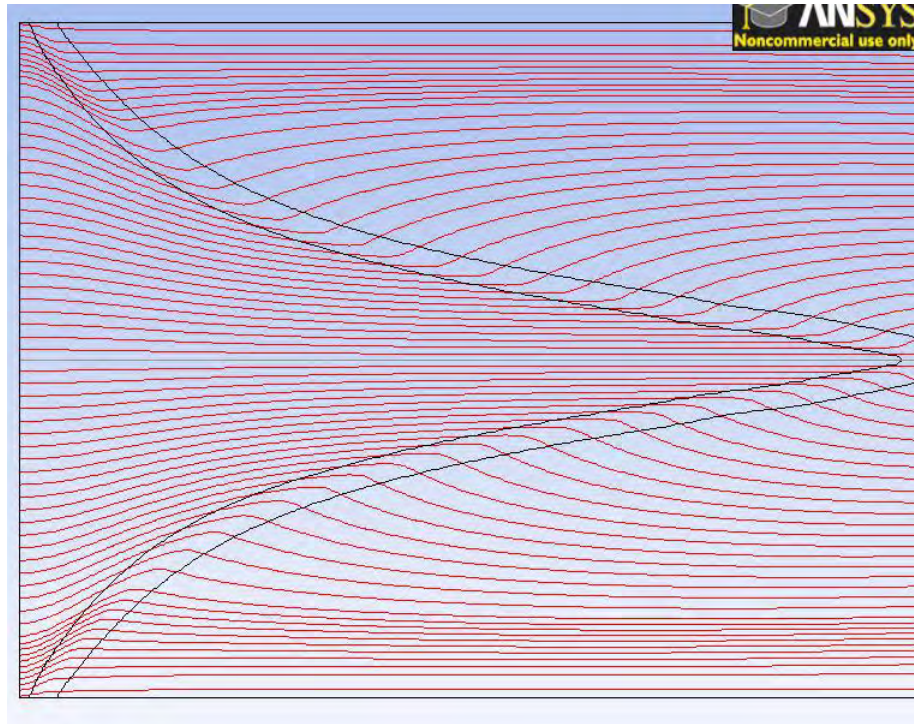ϕ=1.0, v_{in}=0.60 m/s

Figure 4-19. Velocity streamlines through the flame wave. Methane-air combustion, ϕ=1.0, v_{in}=0.80 m/s

Keeping in mind the lack of variation in either S_L or the wall attachment point through the range of inlet velocities, it follows that one could fairly accurately predict the shape of a methane-air flame in this physical model given only the inlet velocity. This is a useful approach when only approximated results are needed.

4.3 Flame Analysis for Varying Fuels

4.3.1 Stoichiometry Effects

A test case was run for methane combustion with air at lean conditions to compare with the flame characteristics of stoichiometric combustion. Previous work with laminar premixed flames has shown that the laminar flame speed is lower at lean conditions versus stoichiometric conditions (Liu et al., 2010a). The temperature contours

for the lean combustion simulation of methane can be seen in Figure 4-20, while the

surfaces representing the beginning and end of the flame wave are shown in Figure 4-21.
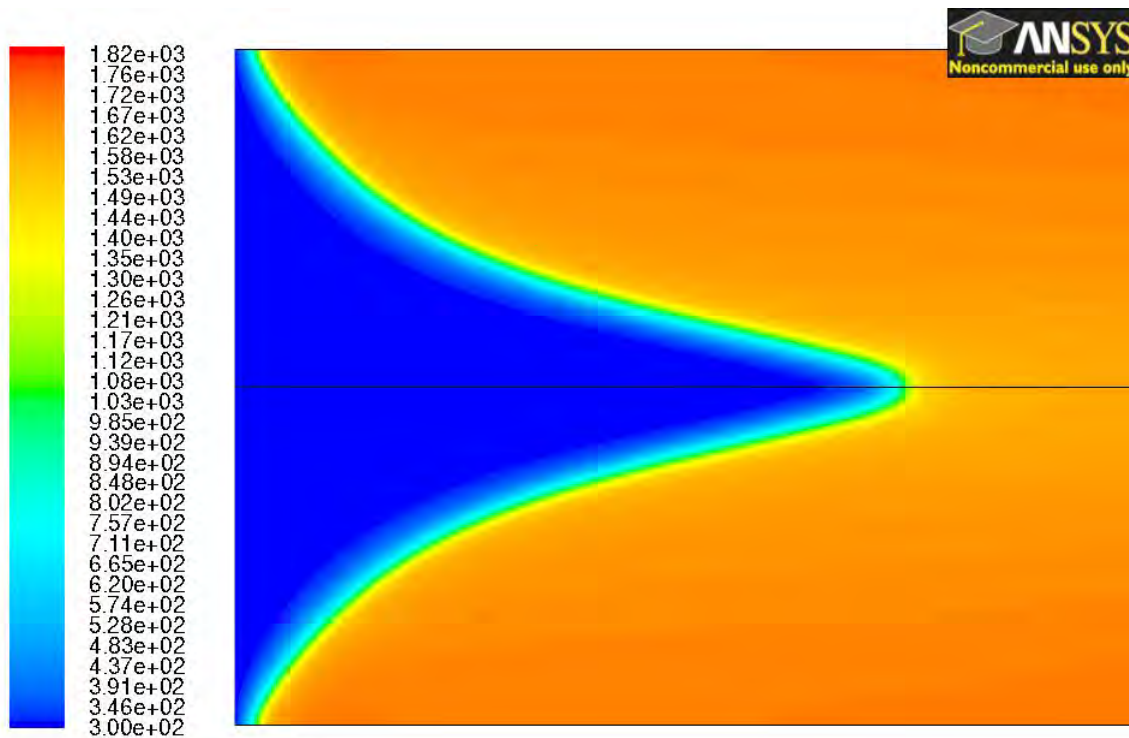

Figure 4-20. Temperature contours for methane-air combustion, ϕ =0.6, v_{in}=0.20 m/s.
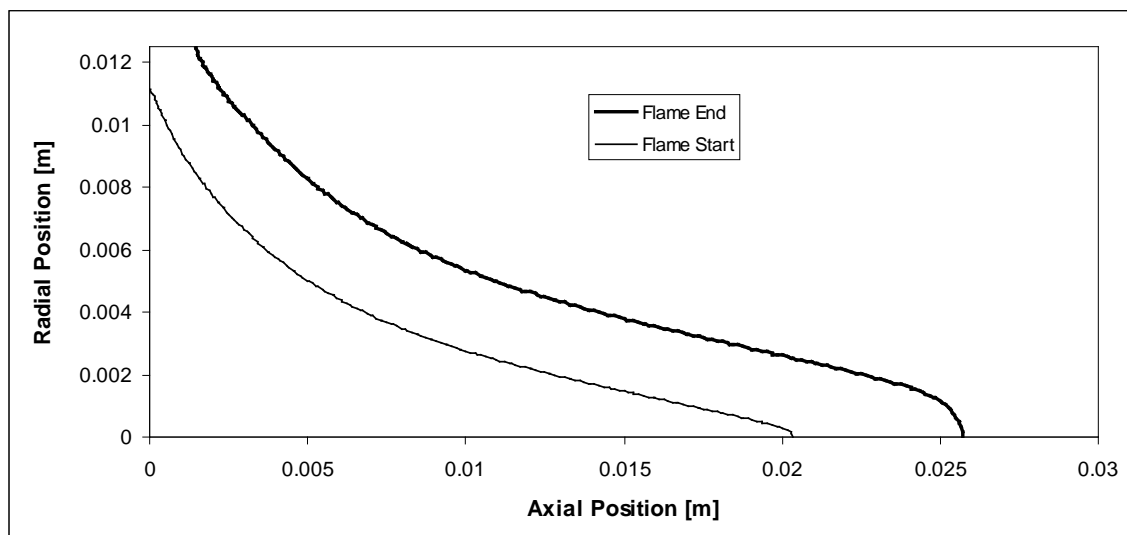
Figure 4-21. Surfaces representing the beginning and end of the flame wave. Methane-air combustion, ϕ=0.6, v_{in}=0.20 m/s.

It is immediately obvious that the effective laminar flame speed is in fact lower at lean conditions than at stoichiometric conditions, as evidenced by the flame shape and inlet velocity. By Equation 1-5, this means that the overall reaction rate of the lean combustion is lower than that of the stoichiometric combustion, since the thermal diffusivity of the unburned mixture should not vary significantly between lean and stoichiometric conditions. It is also apparent that δ_L is significantly larger at lean conditions than at stoichiometric conditions, as Equation 1-4 would predict. For the results shown in Figures 4-20 and 4-21, S_L and $\delta_{L,a}$ were computed to be 0.12 m/s and 5.4 mm, respectively. The computed value for S_L compares very favorably with previous work, which also predicts a value of 0.12 m/s (Liu et al., 2010a).

When compared with the results in Table 4-1, it is apparent that the change in stoichiometry has a significant effect on the flame wave properties. However, a qualitative comparison shows that the overall flame shape is similar between the lean and stoichiometric cases. For instance, compare Figure 4-1 with Figure 4-20. Both flames

have a conical shape that becomes concave near the wall. The wall attachment location is very close to the inlet in both cases. In fact, the surface indicating the beginning of the flame appears to extend back into the inlet for the lean simulation. This indicates that provisions may need to be taken to prevent the flame from flashing back if this physical model were applied to the real world.

4.3.2 Methane versus Biofuels

The temperature contours for the lean and stoichiometric combustions of *LG*, *SG05*, and *SG50* are shown in Figures 4-22 through 4-27.
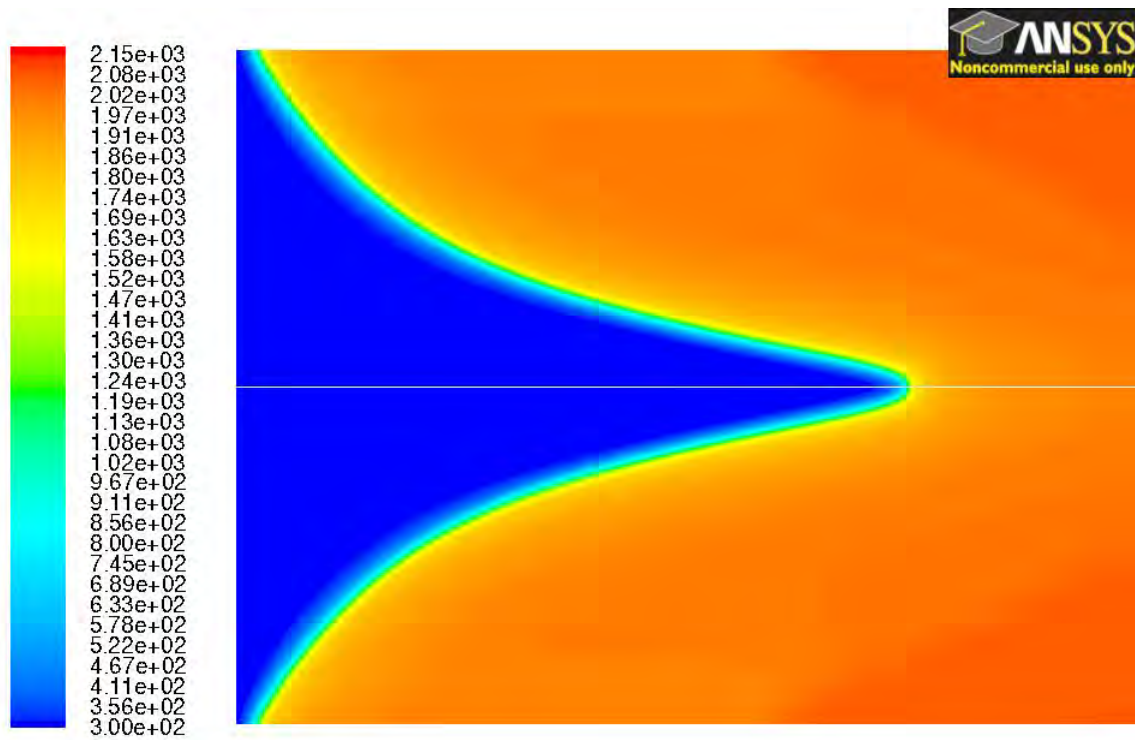

Figure 4-22. Temperature contours for landfill gas (55% CH_4, 45% CO_2) combustion in air, ϕ=1.0, v_{in}=0.40 m/s.

Figure 4-23. Temperature contours for landfill gas (55% CH_4, 45% CO_2) combustion in air, ϕ =0.6, v_{in}=0.15 m/s.

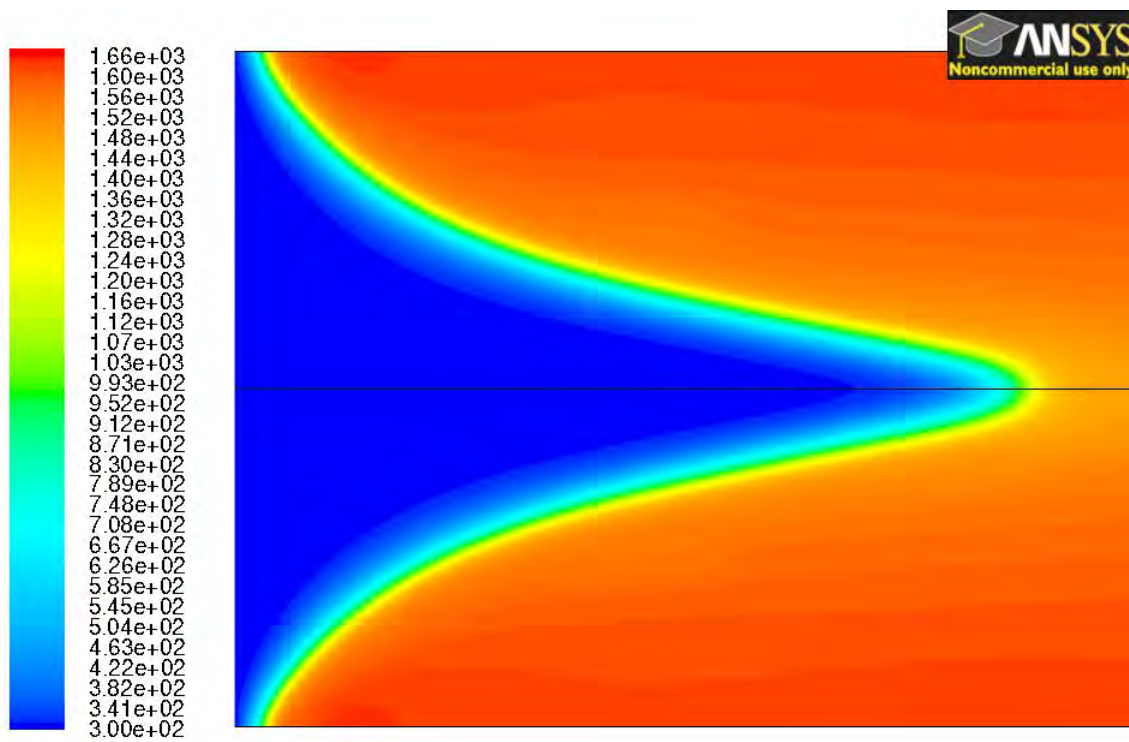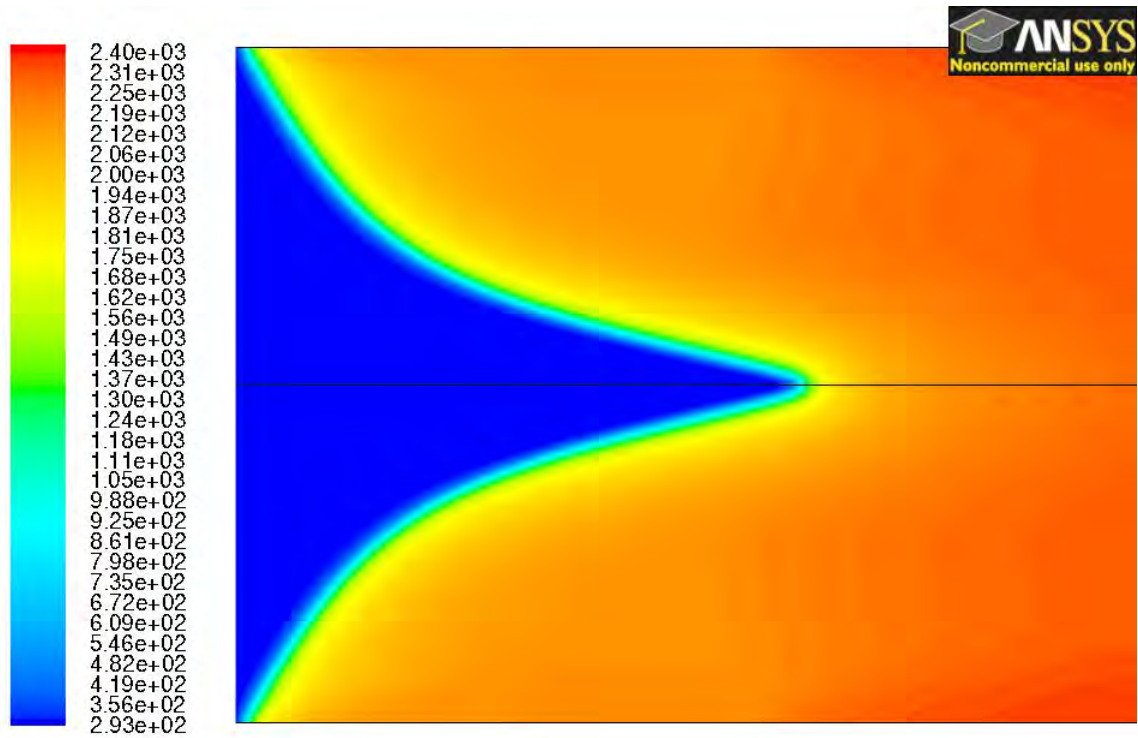Figure 4-24. Temperature contours for syngas (5% H_2, 95% CO) combustion in air, ϕ =1.0, v_{in}=0.70 m/s.
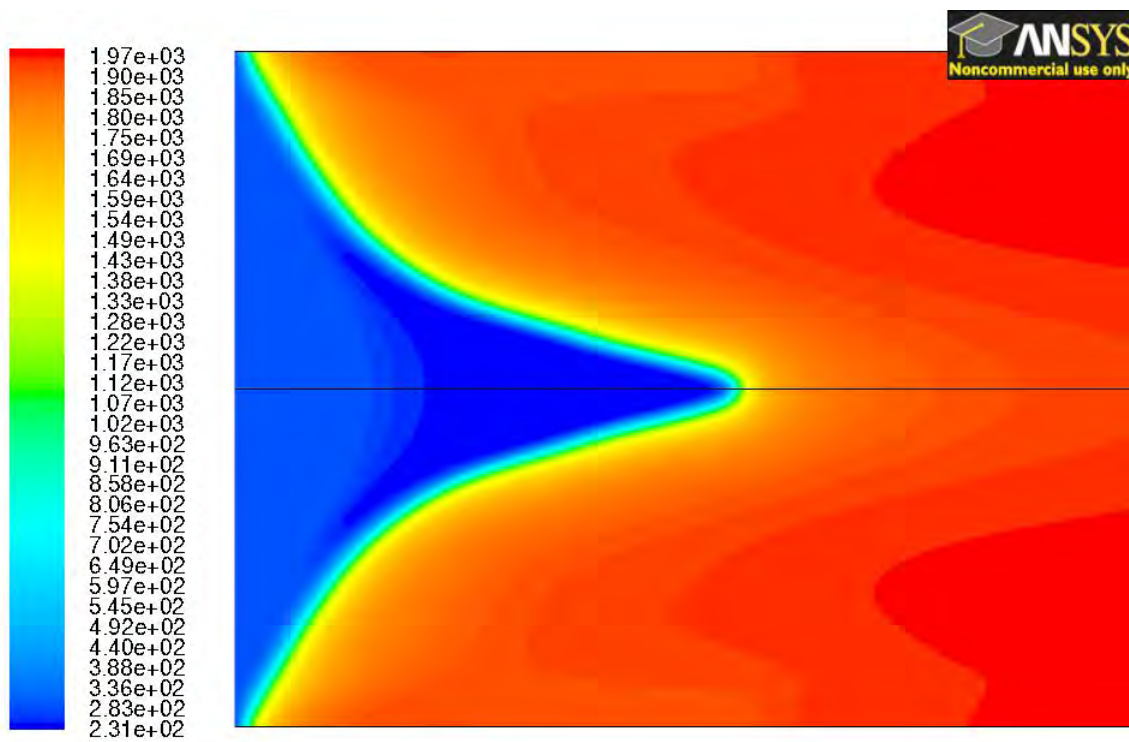
Figure 4-25. Temperature contours for syngas (5% H_2, 95% CO) combustion in air, ϕ =0.6, v_{in}=0.30 m/s.
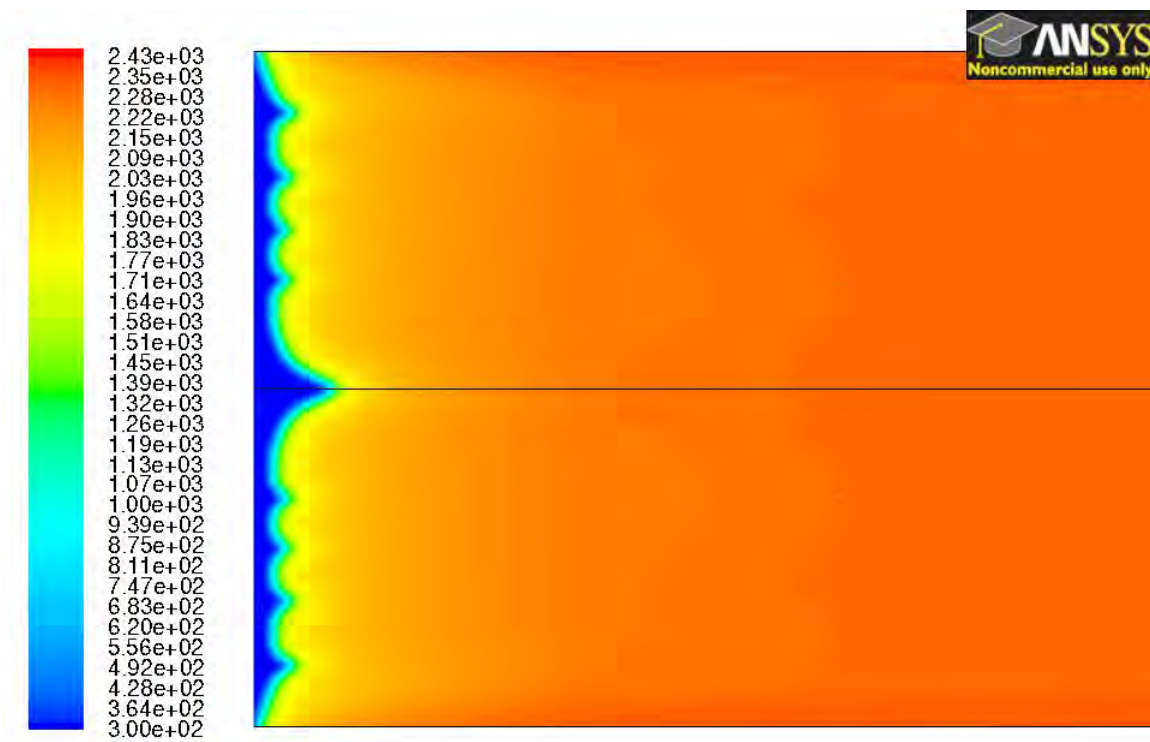
Figure 4-26. Temperature contours for syngas (50% H_2, 50% CO) combustion in air, ϕ =1.0, v_{in}=2.00 m/s.
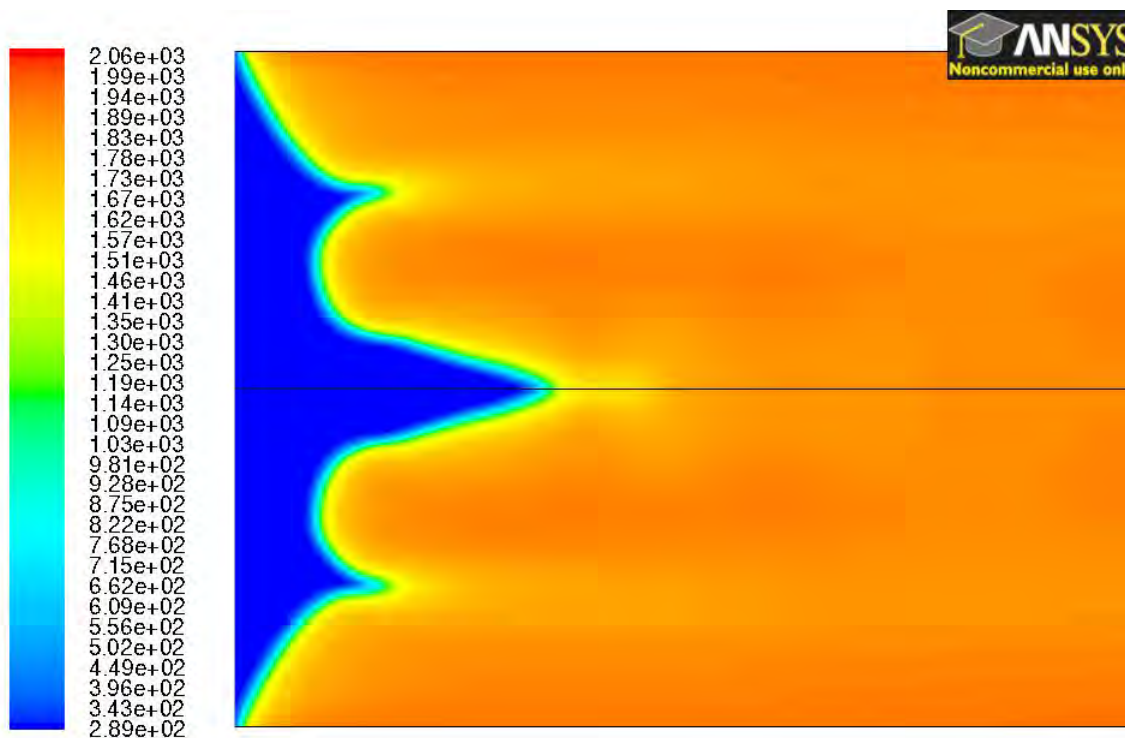
Figure 4-27. Temperature contours for syngas (50% H_2, 50% CO) combustion in air, ϕ=0.6, v_{in}=0.90 m/s.

The flame shapes for *LG* and *SG05* appear to be similar to those seen for methane at both stoichiometric and lean conditions. However, the flame shape for *SG50* appears significantly different for both lean and stoichiometric conditions. The overall shape of the flame is slightly conical, but there are additional peaks in the flame wave between the wall and the axis. It was concluded that the results for *SG50* combustion are most likely non-physical and that it would be presumptuous to interpret the results any further. Acquiring converged solutions proved difficult for simulations with *SG50*. Attempts with varying inlet velocities produced results similar to those seen in Figures 4-26 and 4-27. It is hypothesized that the instabilities seen in the SG50 simulations are a product of numerical difficulties due to the presence of hydrogen. Since hydrogen is a low density species with very high diffusivity, it behaves differently than most other species in the

flame. It is possible that a finer mesh may be able to accurately resolve the numerical instabilities that arise from the presence of hydrogen. This hypothesis could be tested by running the simulations with a finer mesh. However, due to the computational limits of the hardware used for these simulations, this was not pursued at this time.

The results for *SG05* also show some inconsistencies that call the accuracy of the results into question. In both Figures 4-24 and 4-25, it can be seen that the temperature of the unburned gases decreases upstream of the flame front near the axis. In the lean combustion case, the temperature drop is on the order of 70 K. This result does not make any physical sense. Subsequently, caution should be exercised when drawing conclusions from the results. Much like *SG50*, it appears that there is an issue in resolving the kinetics for *SG05*, which is hypothesized to be caused by the presence of hydrogen in the fuel.

Another hypothesis to the inconsistencies seen in the syngas results is that the kinetic mechanism used in this work, GRI version 2.11, is at the root of the problem. After all, there were many improvements made to the GRI mechanism, leading to the release of version 3.0 of the mechanism. In fact, some of the improvements were made to reactions involving elemental hydrogen (Smith et al., 2010). Unfortunately, this hypothesis cannot be tested at present time due to the software limitations of FLUENT.

For both the *LG* cases and the *SG05* cases, the flame properties S_L and $\delta_{L,a}$ were computed and are summarized in Table 4-2.

Table 4-2. Flame characteristics for biofuel-air flames.

Fuel	Φ	v_{in} [m/s]	S_L [m/s]	$\delta_{L,a}$ [mm]
LG	1.0	0.40	0.24	2.48
LG	0.6	0.15	0.08	8.33
SG05	1.0	0.70	0.46	0.97
SG05	0.6	0.30	0.21	0.80

The laminar flame speed for *LG* appears lower than that for methane at both stoichiometric and lean conditions. The results in Table 4-2 agree with other work that predict S_L for *LG*-air combustion at $\phi = 1.0$ and at $\phi = 0.6$ to be 0.23 m/s and 0.08 m/s, respectively (Liu, et al., 2010a). Subsequently, the *LG* flames are thicker than the corresponding methane flames, as would be expected. For the *LG* flame results, the relationship in Equation 1-4 hold true. For the lean *SG05* combustion, both S_L and $\delta_{L,a}$ are lower than the results for stoichiometric *SG05* combustion. Since the majority of the unburned mixture is air, the thermal diffusivity should not vary significantly between the lean and stoichiometric cases, meaning that S_L and $\delta_{L,a}$ should be inversely proportional for both *SG05* simulations. This again calls into question the accuracy of the *SG05* simulations.

The main goal of these tests was to compare the combustion waves resulting from the biofuels with those resulting from methane. There are some conclusions that can be drawn in this avenue. The most telling result is that the general flame shape produced by the biofuels is similar to the flame produced by methane. This is evident for both the *LG* combustion and the *SG05* combustion, although caution should be exercised with regards to the *SG05* results. Also, the flame attachment point showed no dependence on the fuel. Lastly, the flames produced by *LG* combustion followed the results of the methane simulations in that the tube geometry did not affect the laminar flame speed.

4.3.3 Air Oxidation versus O_2/CO_2 Oxidation

The temperature contours for the stoichiometric combustion of methane, *LG*, and *SG05* with the O_2/CO_2 blend are shown in Figures 4-28, 4-29, and 4-30.
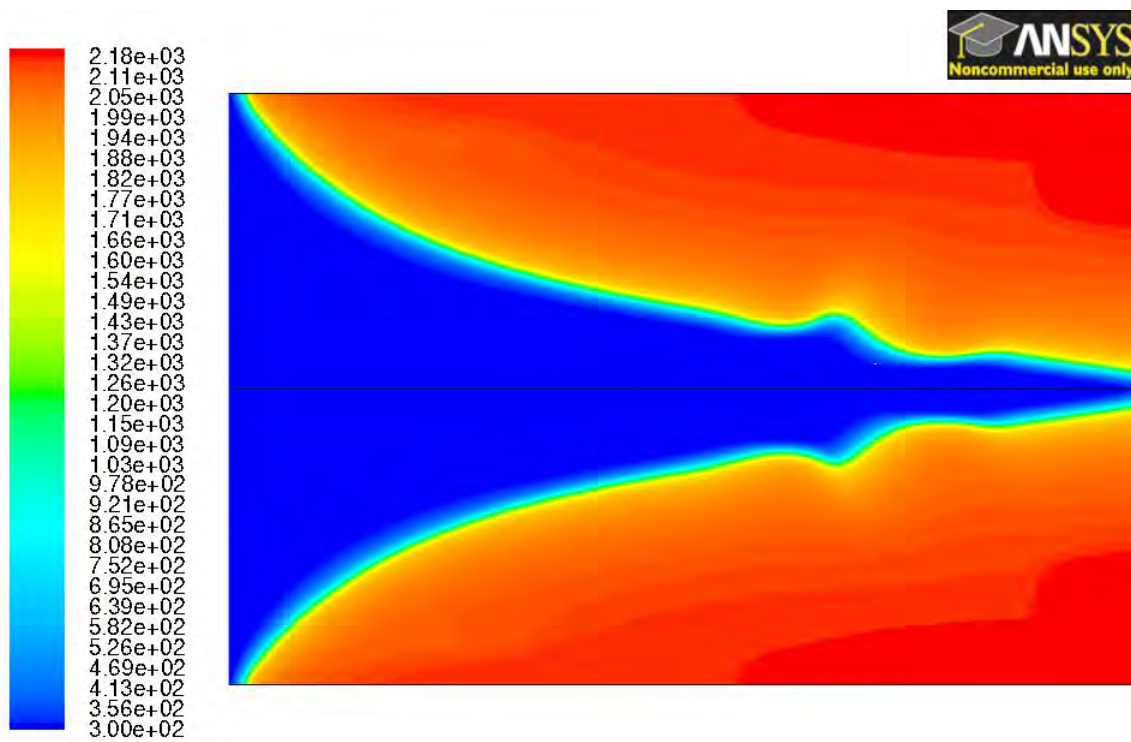
Figure 4-28. Temperature contours for methane combustion in an O_2/CO_2 mixture (30% O_2, 70% CO_2), ϕ =1.0, v_{in}=0.40 m/s.
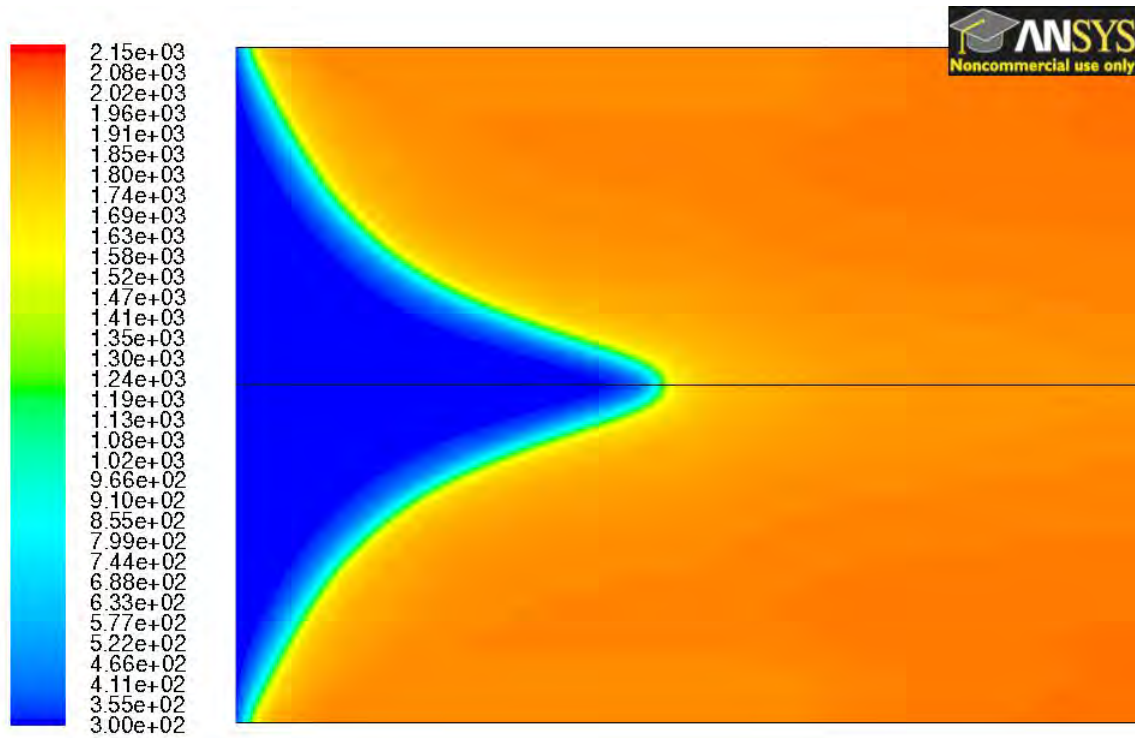
Figure 4-29. Temperature contours for landfill gas combustion in an O_2/CO_2 mixture (30% O_2, 70% CO_2), ϕ =1.0, v_{in}=0.15 m/s.
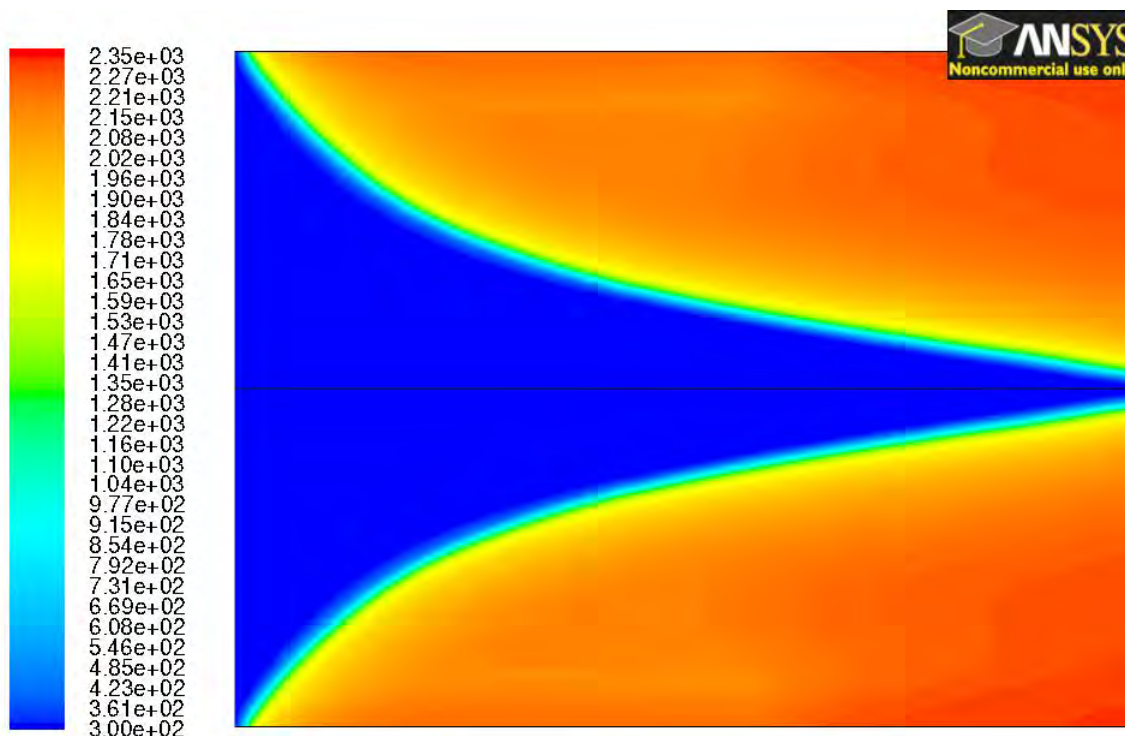
Figure 4-30. Temperature contours for syngas (5% H_2, 95% CO) combustion in an O_2/CO_2 mixture (30% O_2, 70% CO_2), ϕ =1.0, v_{in}=0.70 m/s.

As can be seen in Figures 4-28 and 4-29, the laminar flame speed for both methane and LG is lower than the inlet velocity. Considering that the inlet velocity was set to a value less than S_L computed for stoichiometric combustion of the respective fuel with air, it is clear that the laminar flame speed decreased substantially for both fuels due to changing the composition of the oxidizer. The fact that the laminar flame speed decreased can readily be explained by the relationship in Equation 1-5. Partly due to the thermal diffusivity of carbon dioxide being lower than the thermal diffusivity of nitrogen, the overall thermal diffusivity of the unburned fuel-oxidant mixture decreased when O_2/CO_2 was used as the oxidizer. For example, the thermal diffusivity of the unburned stoichiometric mixture of methane and air was 2.17x10^{-5} m^2/s while the thermal diffusivity for the stoichiometric methane-O_2/CO_2 mixture was 1.42x10^{-5} m^2/s. Since

both carbon dioxide and nitrogen have minimal affect on the reaction rate seen in Equation 1-5, the decrease in thermal diffusivity leads to a decrease in the laminar flame speed.

The results for the combustion of *SG05* with O_2/CO_2 are somewhat peculiar given the results seen in the preceding section. There is no decrease in temperature upstream of the flame wave along the axis as was seen in Figures 4-24 and 4-25. Whatever was causing that problem with the previous syngas simulations no longer appears to come into play once the oxidizer was switched from air to the O_2/CO_2 mixture. This certainly serves as a clue in determining what the underlying issue was in the *SG05*, and possibly the *SG50*, simulations. In essence, the difference between the *SG05*-air simulations and the *SG05*-O_2/CO_2 simulation was that the bulk N_2 was replaced with CO_2. This appears to indicate that there may have been an issue with the chemical kinetics involving nitrogen. Interestingly enough, one of the improvements made to the GRI mechanism between version 2.11 and version 3.0 was changes to the kinetics governing the formation of *NO* (Smith et al., 2010).

Another result that is apparent in Figures 4-28 through 4-30 is that the general flame shape is not affected by changing the oxidizer from air to the O_2/CO_2 mixture. Although some flame characteristics change, the overall conical flame shape seen in the previous test cases is maintained. This implies that the design of premixed burners would not need to change significantly to accommodate this combustion technique.

CHAPTER 5: CONCLUSIONS AND RECOMMENDATIONS

5.1 Summary and Conclusions

A computational study on two-dimensional laminar premixed combustion has been conducted. A working model was developed that fully coupled a comprehensive chemical kinetic mechanism (GRI version 2.11) with computational fluid dynamics in the commercial software program FLUENT. The physical model for the simulations consisted of an adiabatic tube with a constant velocity inlet and an atmospheric pressure outlet. For all cases, the flame waves were shown to be stabilized by the developing boundary layer near the inlet.

The combustion of methane with air was studied in depth and compared with the combustion of three different biofuels: landfill gas and two varieties of syngas. Additionally, combustion with a mixture of 30% O_2 and 70% CO_2 (on a molecular basis) as an oxidizer was proposed as a way to facilitate carbon dioxide capture and sequestration. Flames produced by this combustion technique were then compared with traditional combustion oxidized with air.

Results for methane combustion compared closely with experimental work and one-dimensional numerical work in predicting flame shape, laminar flame speed, and flame thickness. It was shown that the presence of the tube wall affected the flame thickness, but not the laminar flame speed, at sufficiently high inlet velocities.

The computational model was able to accurately model the combustion of landfill gas. It was shown that the laminar flame speed for landfill gas is lower than methane and that the flame shape produced by landfill gas combustion is similar in nature to that of methane. Simulations of syngas combustion proved to be troublesome for the computational model, which struggled to converge to reasonable solutions. Possible explanations for this center around the inability of the model to accurately model the

behavior of hydrogen. This issue could be addressed by increasing the resolution of the finite volume mesh or using a newer kinetic mechanism.

Results from combustion simulations with the O_2/CO_2 oxidizer revealed that the flame characteristics were affected by the lower thermal diffusivity of the oxidizer, resulting in lower laminar flame propagation speeds and thicker combustion waves. The flame shape remained similar to combustion with air.

Across all simulations, laminar flame speed was shown to be solely a function of the fuel-oxidizer mixture properties, which underscored its importance in laminar premixed combustion study. The flame shape similarities between methane and both landfill gas and O_2/CO_2 combustion implies that premixed burner design would not need to change significantly to accommodate these variations. The effects of landfill gas and O_2/CO_2 combustion were found to be similar to the effects of changing stoichiometry.

<div align="center">5.2 Recommendations and Future Work</div>

The main accomplishment of the work presented in this thesis was the development and proof of a working computational model fully coupling a comprehensive kinetic mechanism with commercial CFD software. The difficulties that were encountered in acquiring reasonable solutions goes to show that improvements are still needed in numerical techniques to model combustion to a high level of detail. The test cases that were run with this model and the results that were analyzed merely scratched the surface of the potential work with this type of analysis. By exploring the detailed combustion phenomenon in two-dimensions versus the one-dimensional analysis that is often studied, there are many additional topics that can be explored. Some examples include examining the effects of fuel additives on the flame structure and examining a co-flow arrangement with a shielding gas to study the conditions which result in flame quenching. Additionally, different physical models could be studied to investigate improvements to burner design.

From a more practical standpoint, it would be useful to re-examine this work using a more recent chemical kinetic mechanism, such as GRI version 3.0 or the San Diego mechanism, once software limitations are addressed to allow for such work. Also, more work needs to be done with the simulations (and validation of the results) of syngas combustion to better understand the difficulties encountered with those simulations in this work.

REFERENCES

Andersen, J.W. and Fein, R.S. 1950. "Measurement of Normal Burning Velocities of Propane-Air Flames from Shadow Photographs." *Journal of Chemical Physics* 18: 441-443.

Anderson Jr., J.D. 1995. *Computational Fluid Dynamics: The Basics with Applications*. New York: McGraw-Hill, Inc.

Ashforth, G.K., Long, R., and Garner, F.H. 1950. "Determination of Burning Velocities from Shadow and Direct Photographs of Flame." *Journal of Chemical Physics* 18: 1112-1113.

Bade Shrestha, S.O. and Narayanan, G. 2008. "Landfill gas with hydrogen addition – A fuel for SI engines." *Fuel* 87: 3616-3626.

Bilger, R.W, Starner, S.H., Kee, R.J. 1989. "On Reduced Mechanisms for Methane – Air Combustion in Nonpremixed Flames." *Combustion and Flame* 80: 135-149.

Botha J.P. and Spalding, D.B. 1954. "The Laminar Flame Speed of Propane/Air Mixtures with Heat Extraction from the Flame." *Proceedings of the Royal Society of London. Series A, Mathematical and Physical Sciences* 225, 71-96.

Bowman, C.T., Hanson, R.K., Davidson, D.F., Gardiner, Jr., W.C., Lissianski, V., Smith, G.P., Golden, D.M., Frenklach, M., and Goldenberg, M. 1995. *GRI-MECH 2.11*. Retrieved May 25th 2010 from http://www.me.berkeley.edu/gri_mech/

Brokaw, R.S., 1967. "Ignition Kinetics of the Carbon Monoxide-Oxygen Reaction." *Eleventh Symposium (Int.) on Combustion* 1063-1073.

Curran, H. J., P. Gaffuri, W. J. Pitz, and C. K. Westbrook. 2002. "A Comprehensive Modeling Study of iso-Octane Oxidation." *Combustion and Flame* 129: 253-280.

Dudgeon, R.J. 2009. "An Exergy-Based Analysis of Gasification and Oxyburn Processes." Master's Thesis, The University of Iowa.

El-Mahallawy, F. and Habik, S.E.D. 2002. *Fundamentals and Technology of Combustion*. Amsterdam: Elsevier.

Feldick, A.M. 2007. "Numerical Investigation of Intermediate Temperature Auto-Ignition." Master's Thesis, The University of Iowa.

FLUENT. 2009. "Theory Guide: Release 12.0." Last modified January 23, 2009.

Gayden, A.G., and Wolfhard, H.G. 1960. *Flames: Their Structure, Radiation and Temperature (2nd Ed.)*. London: Chapman and Hall.

Glassman, I. and Yetter, A. 2008. *Combustion*. Amsterdam: Elsevier.

Gordon, S. and McBride, B.J. 1994. "Computer Program for Calculation of Complex Chemical Equilibrium Compositions and Applications." *NASA Reference Publication* 1311.

Hawkes, E.R and Chen, J.H. 2004. "Direct Numerical Simulation of Hydrogen-Enriched Lean Premixed Methane-Air Flames." *Combustion and Flame* 138: 242-258.

Ho, M.T, Allinson, G., and Wiley, D.E. 2006. "Comparison of CO_2 separation options for geo-sequestration: are membranes competitive?" *Desalination* 192: 288-295.

Kearns, D.T. and Webley, P.A. 2004. "Application of an adsorption non-flow exergy function to an exergy analysis of a pressure swing adsorption cycle." *Chemical Engineering Science* 59: 3537-3557.

Kee, R.J., Rupley, F.M., Miller, J.A., Coltrin, M.E., Grcar, J.F., Meeks, E., Moffat, H.K., Lutz, A.E., Dixon-Lewis, G., Smooke, M.D., Warnatz, J., Evans, G.H., Larson, R.S., Mitchell, R.E., Petzold, L.R., Reynolds, W.C., Caracotsios, M., Stewart, W.E., Glarborg, P., Wang, C., Adigun, O., Houf, W.G., Chou, C.P., Miller, S.F., Ho, P., and Young, D.J. 2004. *CHEMKIN Release 4.0*. Reaction Design Inc., San Diego.

Kuo, Kenneth K. 2005. *Principles of Combustion*. New York: John Wiley and Sons.

Lewis, B. and von Elbe, G. 1961. *Combustion, Flames and Explosions of Gases (2nd Ed.)*. New York: Academic Press.

Liu, C., Yan, B., Chen, G., and Bai, X.S. 2010a. "Structures and burning velocity of biomass derived gas flames." *International Journal of Hydrogen Energy* 35: 542-555.

Liu, K., Song, C., and Subramani, V. 2010b. *Hydrogen and Syngas Production and Purification Technologies*. New York: John Wiley and Sons.

Mallard, E. and Le Chatelier, H.L. 1883. "Thermal Model for Flame Propagation." *Annales des Mines* 4: 379.

McLean, I.C., Smith, D.B., and Taylor, S.C. 1994. "The Use of Carbon Monoxide/Hydrogen Burning Velocities to Examine the Rate of the CO + OH Reaction." *Twenty-Fifth Symposium (International) on Combustion* 749-757.

Moran, M.J., and Shapiro, H.N. 2008. *Fundamentals of Engineering Thermodynamics: Fifth Edition.* New York: John Wiley and Sons.

Pitsch, H. and Steiner, H. 2000. "Large-Eddy Simulation of a Turbulent Piloted Methane/Air Diffusion Flame (Sandia Flame D)." *Physics of Fluids* 12: 2541-2554.

Powling, J. 1949. "A new burner method for the determination of low burning velocities and limits of inflammability." *Fuel* 28: 25.

Smith, G.P., Golden, D.M., Frenklach, M., Moriarty, N.W., Eiteneer, B., Goldenberg, M., Bowman, C.T., Hanson, R.K., Song, S., Gardiner Jr., G.C., Lissianski, V., and Qin, Z., *GRI-MECH 3.0*. Retrieved May 25th 2010 from http://www.me.berkeley.edu/gri_mech/

Sorensen, J.N. and Loc, T.P. 1989. "High Order Axisymmetric Navier-Stokes Code: Description and Evaluation of Boundary Conditions." *International Journal for Numerical Methods in Fluids* 9: 1517-1537.

U.S. Energy Information Administration (EIA). 2010. *Annual Energy Review 2009*. *DOE/EIA-0384(2009)*.

Vagelopoulos, C.M. and Egolfopoulos, F.N. 1998. "Direct Experimental Determination of Laminar Flame Speeds." *Twenty-Seventh Symposium (International) on Combustion* 513-519.

Warnatz, J. 1981. "The Structure of Laminar Alkane-, Alkene-, and Acetylene Flames." *Eighteenth Symposium (Int.) on Combustion* 369-384.

Weinberg, F.J. 1963. *Optics of Flames*. London: Butterworths.

Westbrook, C.K., and Dryer, F.L. 1981. "Chemical Kinetics and Modeling of Combustion Processes." *Eighteenth Symposium (Int.) on Combustion* 749-767.

Yeoh, G.H. and Yuen, K.K. 2009. Computational Fluid Dynamics in Fire Engineering: Theory, Modelling and Practice. Amsterdam: Elsevier.